BIDIRECTIONAL REGULATION OF MIGRATION AND CHEMOTAXIS BETWEEN MONOCYTES AND TUMOR CELLS

By

Wenxuan Du

A thesis submitted to the Johns Hopkins University in conformity with the requirements for the degree of Master of Science in Engineering

Baltimore, Maryland

May 2020

Abstract

The dissemination of primary cancer cells to distal sites of patient body, namely metastasis, accounts for almost 90% of all cancer-related deaths over the world. Triple negative breast cancer (TNBC) is one of the most metastatic cancer subtypes. Without available targeted therapies due to lack of estrogen receptor (ER), progesterone receptor (PR) and HER2 receptor, the five-year survival rate of TNBC patients is down to 77% in contrast with 93% of those diagnosed with other breast cancer subtypes.

Tumor infiltrating macrophages have been shown to associate with poor prognosis of TNBC. Known for their plasticity and immunomodulatory effects, macrophages infiltrated into tumor center and invasive margin have been identified as tumor associated macrophages (TAMs) considering their specific tumor-promoting phenotypes after re-education. Circulating monocytes in the peripheral blood are the main source of TAM infiltration in tumor sites. Nevertheless, the migration behavior of monocytes in tumor stroma has long been neglected due to the complexity of setting up proper *in-vitro* 3D cell migration assays.

This study explores the regulation of monocyte migration by highly metastatic TNBC cell line MDA-MB-231 via elaborated 3D extracellular matrix gel model. We identify two separated migration patterns during monocytes' recruitment process, namely enhanced migration and biased migration. We show that breast cancer cells facilitated recruitment of monocytes to tumor bulk via a combination of IL6-dependent enhanced migration and CCL2-dependent biased migration. Tocilizumab treatment of IL6R blocking significantly reduced cancer cells' migration increasing effect on monocytes and thus minimizing later TAM infiltration.

The study further explores in return the regulation of cancer cell migration by re-educated macrophages using a more physiological relevant 3D double-layer co-culture spheroid system.

We show increased invasion of cancer cells with assistance of TAMs and provide an insight into inhibiting monocyte migration as an immunotherapy against cancer metastasis.

Primary Reader and Advisor: Denis Wirtz

Secondary Reader: Pei-Hsun Wu

Acknowledgments

This thesis can’t do without the precious encourage, support and guidance form my advisor, colleagues, family and friends.

I would like to thank my advisor Dr. Denis Wirtz whose lad I have devoted myself to for the past two years. Dr. Wirtz offered me the opportunity to join his prominent lab as a novice in onco-immunology with extremely limited experience on cell migration studies. The project I have been working on is promising, challenging and fulfilling. It is under the guidance of Dr. Wirtz that I was able to push forward the project and make exciting discoveries.

I would also like to thank every member in Wirtz lab for their supportive and encouraging characters. Talking science with all of you guys always made the best of my days. Special thanks to Dr. Michael Harris who brought me in the lab and taught me all relevant biology techniques from the ground. I wish you all good in your industry life. Finally, I would like to appreciate Dr. Pei-Hsun Wu’s help for agreeing on being my second thesis reader.

Table of Contents

List of Figures

1. Introduction

1.1 Re-education of monocytes into tumor associated macrophages

Classification of macrophages is never easy due to their intricate origins and functions. One of the most successful and widely adopted classification is the mononuclear-phagocytic system (MPS)[1]. In the NPS system, mature adult macrophages are polarized and differentiated from circulating monocytes in peripheral blood which originate from the myeloid precursors in the bone marrow. This postnatal definition of monocytes and macrophages can't be applied to tissue-resident macrophages that normally have prenatal origins[2]. For instance, microglial cells in central nervous system are derived from yolk sac, and Langerhans cells in liver are originated from fetal liver.

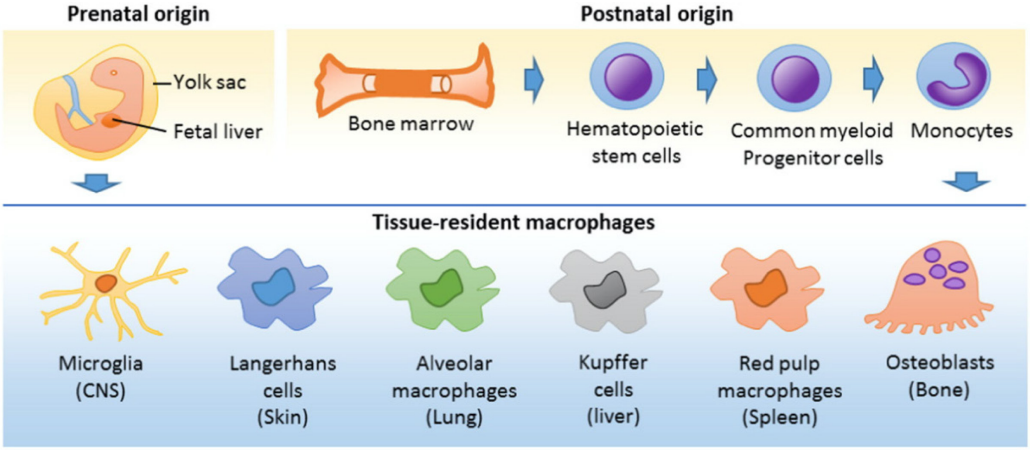

Figure 1: Origins of recruited macrophages and tissue-resident macrophages[2]. Tissue-resident macrophages have prenatal origins while normal recruited and differentiated macrophages have postnatal origins from hematopoietic stem cells in the bone marrow.

Circulating monocytes can be further classified as classical (high expression of CD14) and non-classical (low expression of CD14 and additional co-expression of CD16) monocytes[3]. Classical monocytes are known to be recruited to various tissue sites and later differentiate into macrophages according to environmental cues during inflammations. To define functions of these monocyte-derived macrophages, another linear-scale classification system based on their activation status has been developed[4]. M1-like macrophages, also known as classically activated

macrophages, are usually induced by stimuli like LPS and IFN-γ and are capable of secreting pro-inflammatory cytokines to help eliminate pathogens in body. While in the other hand, M2-like macrophages, also known as alternatively activated macrophages, are usually induced by stimuli like IL4, IL13, TGF-β and usually come with immunosuppressive modulation, inflammation resolution and tissue repair[5]. Under a cancer circumstance, monocytes recruited to solid tumor bulk can be re-educated by cancer cells via either secreted soluble factors or cell-cell interactions into a specific phenotype called tumor associated macrophages (TAMs). Although M1/M2 classification is not sufficient enough to describe the phenotype of tumor associated macrophages, it has been shown that TAMs resemble M2-like macrophages as they are found to be immunosuppressive and unable to produce pro-inflammatory cytokines for tumor cell killing. As a result, in most studies, M2-like macrophage markers like CD163, CD206 are commonly used as markers for TAMs.

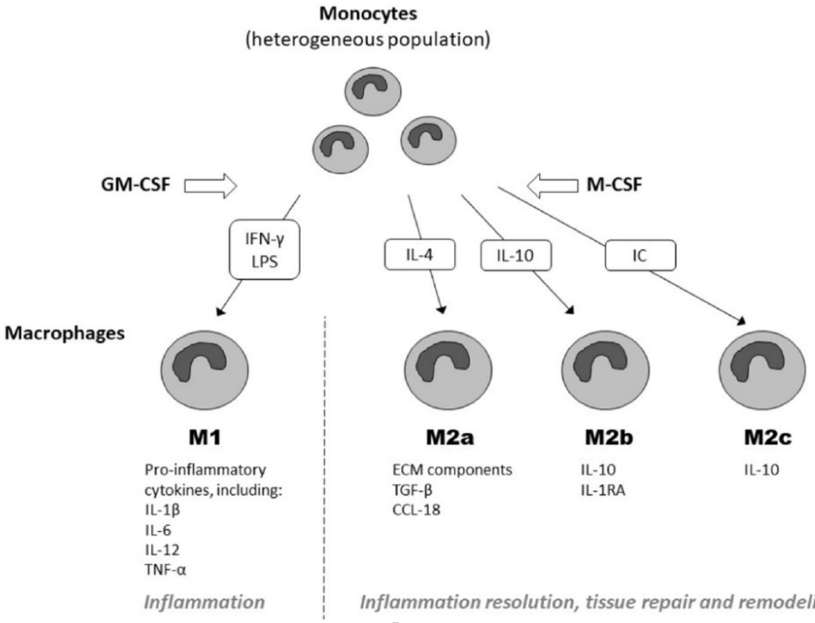

Figure 2: M1/M2 classification of macrophages[5]. M1-like macrophages secrete pro-inflammatory cytokines like IL1β and TNF-α. M2-like macrophages are related with inflammation resolution, tissue repair and remodeling.

1.2 Tumor associated macrophages exhibit tumor-promoting effects

Tumor associated macrophages comprise a considerable fraction of cell mass in solid tumors. Clinical outcomes have shown a clear correlation between M2-like TAMs infiltration and poor prognosis of patients. Previous work done by Tiia J. Honkanen *et al* explored macrophage and Treg infiltrations of $HER2^+$ breast cancer through immunohistochemistry[6]. As is shown in figure 3 below, there existed a clear enrichment of M2-like TAMs both in center of tumor and invasive margin in contrast with M1-like normal pro-inflammatory macrophages, with a fold change of almost 10. In addition, Kaplan-Meier curves illustrated that existence of $iNOS^+$ M1-like macrophages were associated with better overall survival rate while infiltration of $CD163^+$ M2-like TAMs correlated with worse clinical outcomes.

		Median density (cells/mm²)	Range (cells/mm²)	ROC cut-off value (cells/mm²)
M1-like macrophages (iNOS)	IM	42	4–145	58
	CT	37	4–173	37
M2-like macrophages (CD163)	IM	338	24–957	307
	CT	295	15–983	241
Regulatory T-cells (FoxP3)	IM	145	14–739	134
	CT	92	6–796	82

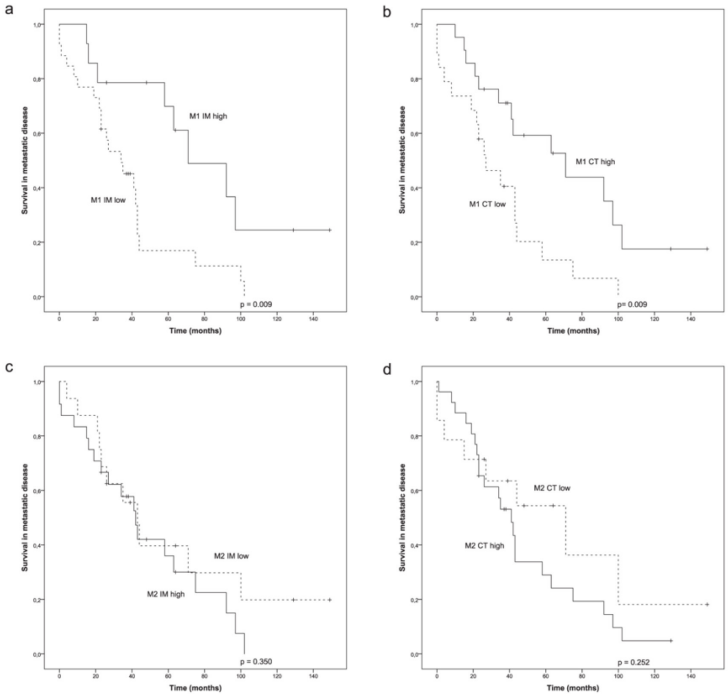

Figure 3: Infiltrated macrophage cell counting via IHC and Kaplan-Meier Curve of M1/M2[6]. IM stands for invasive margin and CT stands for center of tumor. (a-b) High infiltration of M1-like macrophage in tumor center and invasive margin correlated with higher survival rate. (c-d) High infiltration of M2-like TAMs correlated with lower survival rate.

Studies have shown tumor associated macrophages' pro-tumoral effects in a few aspects[7,8]. TAMs are able to initiate neovascularization and activate tumor cells. In the meanwhile, immunosuppression modulated by TAMs will induce regulatory T cells (Treg) and Myeloid-derived suppressor cells (MDSC), hindering the cytotoxic $CD8^+$ T cells' activation. Finally, TAMs help create advantages for tumor cell invasion and metastasis via matrix degradation and pre-metastatic niche establishment[9].

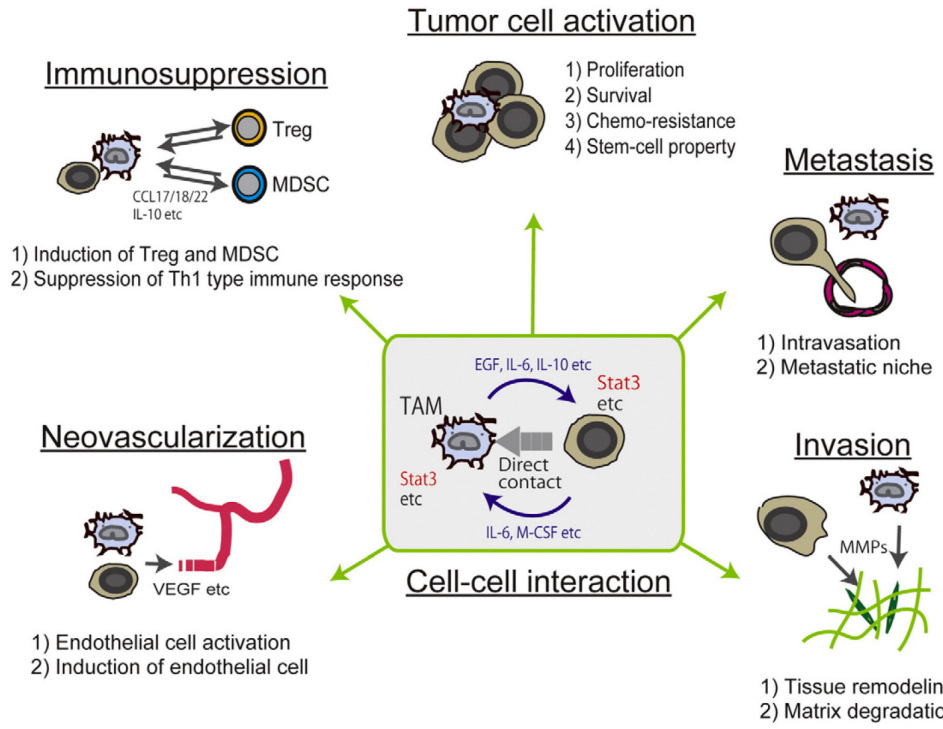

Figure 4: Summary of TAMs' pro-tumoral effects[9]. Tumor associated macrophages are able to induce immunosuppression and neovascularization. Tumor cells are activated by TAMs and their invasion and metastasis get promoted.

1.3 Lack of studies on monocyte migration via 3D cell migration assays

Much significance has been attached on the mechanisms of how tumor cells re-educate monocytes into tumor associated macrophages along with how TAMs promote tumor-genesis and metastasis. However, the prerequisite question about the migration behavior of monocytes in

tumor stroma ECM before infiltration into tumor center and invasive margin has long been neglected.

Worse still, current *in-vitro* migration/chemotaxis assays have serious limitations. Figure 5 below is a summary for all current *in-vitro* migration/chemotaxis assays. Wildly adopted transwell and wound-healing assays can only elucidate collective-cell migration instead of single-cell migration and are far away from 3D migration assay due to lack of ECM. μ-slide chemotaxis assay and ECM coating cell migration assay can only be viewed as a 2.5D in that cell movement in a thin layer of ECM will be limited in the z-axis. Even though ECM 3D gel system has been developed[10,11], very few groups continue to analyze single-cell speed/persistence because it requires a live-cell condition built in microscope for taking long time video, which is very expensive and time-consuming. As a result, it is imperative to develop proper 3D cell migration models for cell migration analysis in a single-cell level.

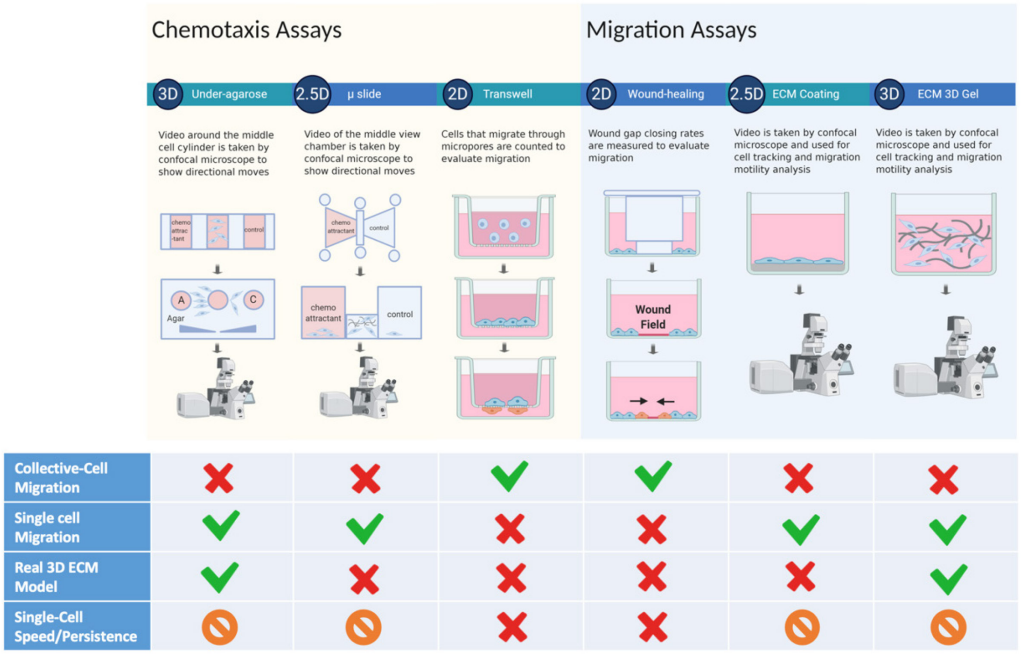

Figure 5: Summary of current *in-vitro* chemotaxis & migration assays. Chemotaxis assays contain under-agarose[12]/μ slide/transwell assays. Migration assays contain wound-healing/ECM coating/ECM 3D gel assays. Only ECM 3D gel and under-agarose assays are real 3D cell migration assays on single-cell level.

1.4 Single cell migration in 3D collagen gel

The most abundant fibrous protein in extracellular matrix in type I collagen[13]. In a three-dimensional (3D) type I collagen gel that supports migration and chemotaxis, we are able to study cells' migratory phenotypes by taking videos for further tracking and analysis. Cells with proper initial density are embedded inside solidified gel with formed collagen fibers so that micro distances exist among cells, enabling singe-cell migration. During migration process, matrix metalloproteinases (MMPs) are secreted and activated by cells to degrade and remodel the ECM matrix[14]. Generation of multigenerational and dendritic pseudopodial protrusions is a hallmark of cell migration in 3D matrix[15]. These protrusions are composed of clustered integrins linking ECM fibers with the intracellular actin network. Previous work done by Anjil Giri *et al* showed that protrusions emerging from the primary cell body are mother protrusions and are controlled through FAK, talin and p130Cas, while protrusions that stem from mother protrusions are regulated by Arp2/3 complex[16]. This collagen type I gel resembles characteristics of collagen-rich stroma of tumor bulk and can easily be used for screening responsible soluble factors via applying conditioned media on top of the gel followed by observing the migratory phenotype change of target cells.

1.5 Density-dependent migration controlled by IL6/IL8 synergistic autocrine pathway

Previous study by Hasini Jayatilaka *et al* showed the cell density effect on highly metastatic MDA-MB-231 cell line. It has been shown that increased cell density in 3D collagen gel resulted in increased motility of cells[17].

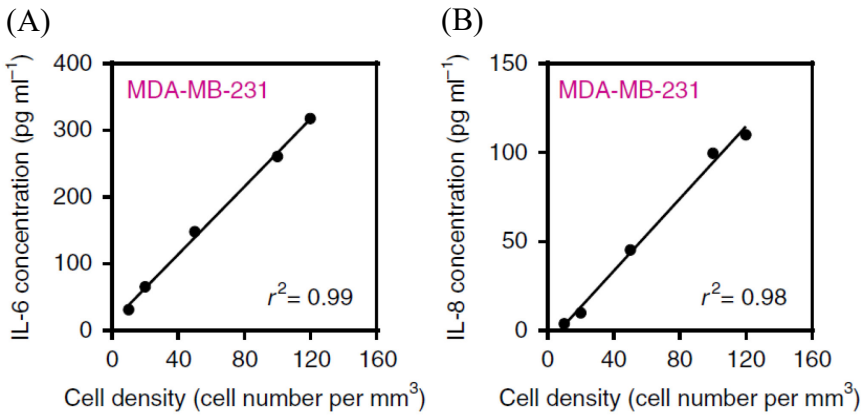

Figure 6: Density-dependent expression of IL6/IL8 from MDA-MB-231[5]. (A) IL6 expression as a function of cell density (n=3). (B) IL8 expression as a function of cell density (n=3).

IL6 and IL8 secretion was found to positively related with cell density and further mechanism study revealed an IL6/IL8 synergistic autocrine pathway functioning through JAK2/STAT3 cascade[17]. Whether this autocrine pathway to enhance migration of tumor cells themselves can work via a paracrine manner to affect monocyte migration in the stroma is interesting to study.

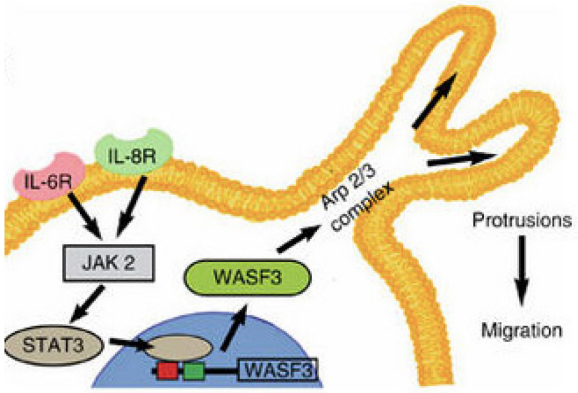

Figure 7: JAK2/STAT3 cascade initiated by synergistic IL6/IL8 pathway[17]. Binding of IL6/IL8 to their respective receptors initiate JAK2/STAT3 cascade that leads to the generation of Arp2/3 complex.

2. Results & Discussion

2.1 Conditioned media from TNBC increases monocyte migration

2.1.1 Conditioned media from TNBC increases U937 migration

To first test if cancer cells can affect migration of monocytes, MDA-MB-231 high metastatic triple negative breast cancer cell line and U937 monocyte cell line were chosen. U937 cells are isolated form histiocytic lymphoma and are widely used to study the differentiation of monocytes into macrophages together with THP-1 cells. U937 cells can be polarized and differentiated in response to various soluble stimuli and then adopt the characteristics and morphologies of mature macrophages.

Conditioned media (CM) from MDA-MB-231 cells were harvested after 48 hours of seeding with adequate soluble factors secretion. To make the most of biological sense, conditioned media were harvested from MDA-MB-231 cells seeded in 3D collagen gel instead of normal 2D cell culture plates to mimic the collagen-rich tumor environment.

(A) (B)

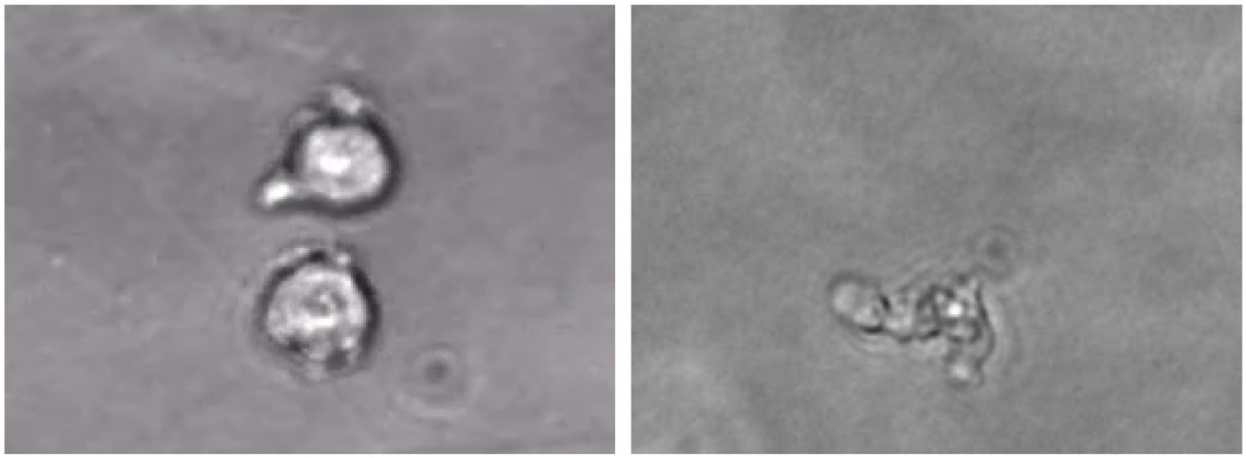

Control (RPMI) MDA-MB-231 WT CM

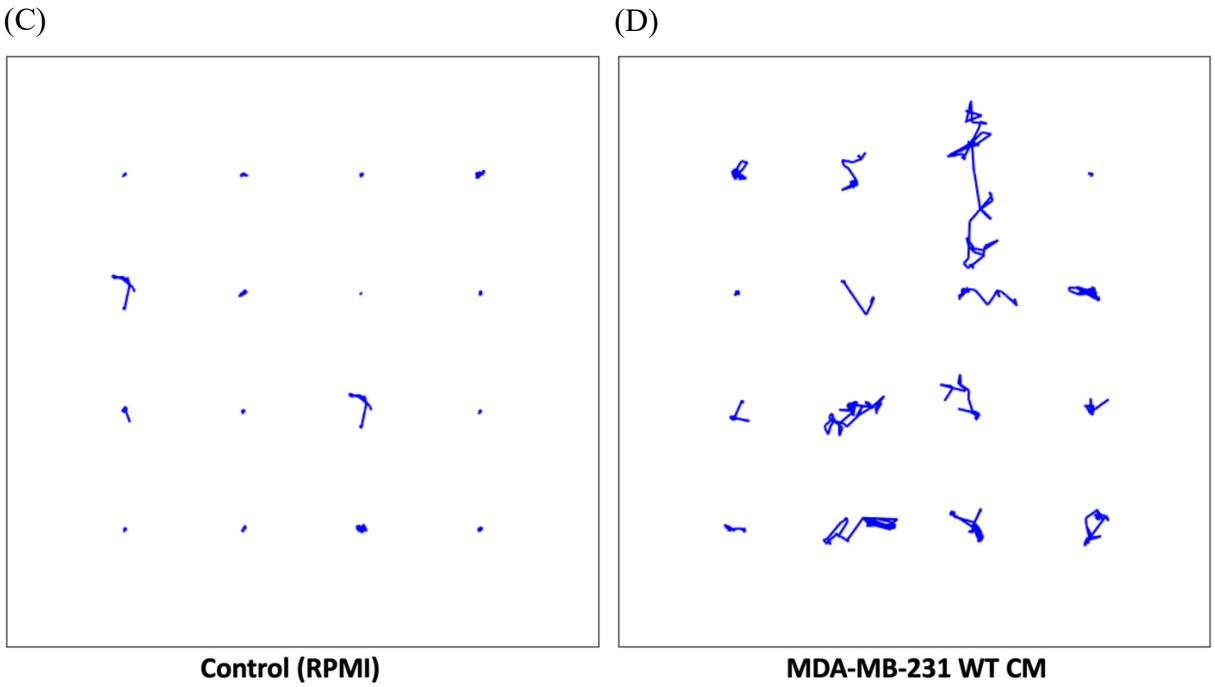

Figure 8: Phase contrast images and trajectories of U937 exposed to MDA-MB-231 CM. (A) 20x phase contrast image of U937 exposed to RPMI fresh media, protrusions were generated. (B) 20x phase contrast image of U937 exposed to MDA-MB-231 CM, ameboid morphology was observed. (C) Random plotting of U937 trajectories exposed to fresh RPMI. (D) Random plotting of U937 trajectories exposed to MDA-MB-231 CM. Cell movements were increased.

Based on figure 8, we can clear see that conditioned media from MDA-MB-231 significantly increased U937 cells' migration inside 3D collagen gel. Morphology changes were observed that U937 cells tended to adopt an ameboid phenotype with increased migration compared to local protrusion generation of control group cells. Using coordinates information obtained from cell tracking, mean square displacement (MSD) values were calculated. Considering an even distribution of soluble factors in the gel without a concentration gradient, U937 cell movements were viewed as random walks and thus an anisotropic persistence random walk (APRW) model[19] previous developed by Pei-Hsun Wu *et al* was applied for further single-cell analysis. As is shown in figure 9, single-cell analysis results confirmed U937 cells' increases of speed, diffusivity, persistence in 3D migration after contact with soluble factors in MDA-MB-231 CM.

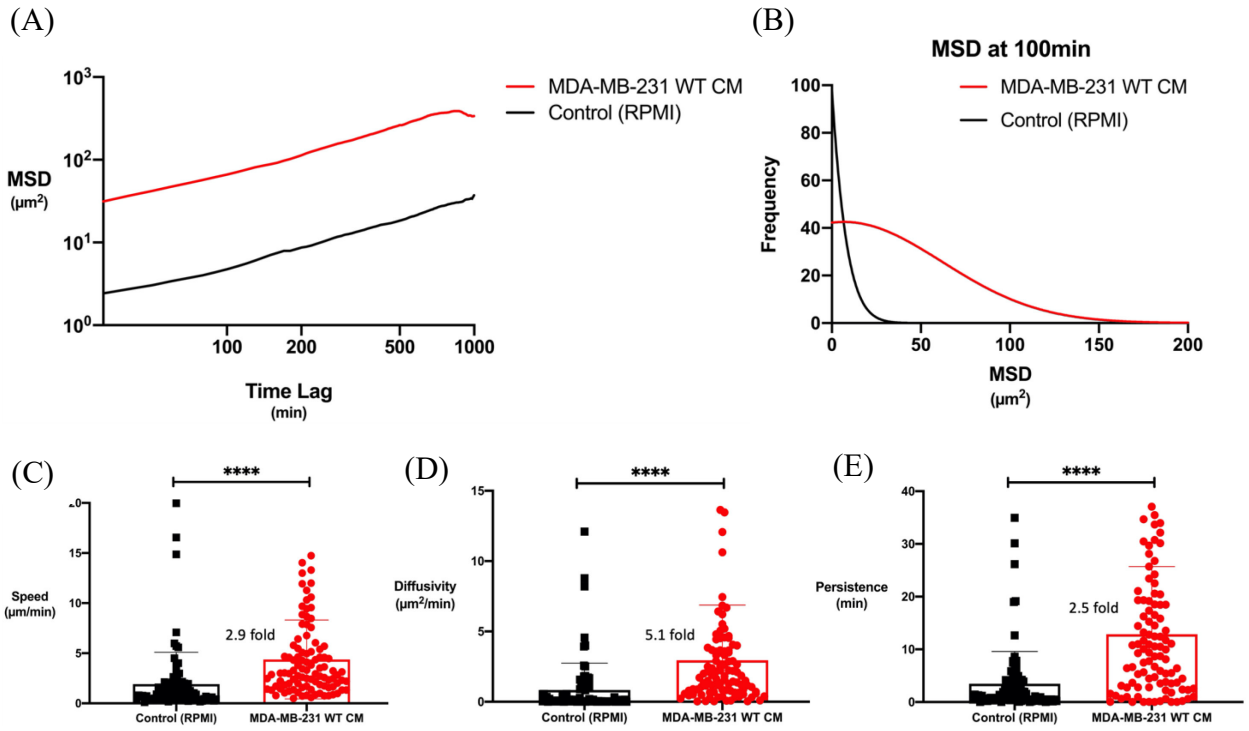

Figure 9: MSD distribution and single-cell analysis of U937 exposed to MDA-MB-231 CM. (A) MSD plotting against time lag. MSDs of all tracked cells were taken average and plotted. U937 cells exposed to MDA CM had larger MSD throughout the whole time period. (B) Non-linear regression of MSD. MSDs of U937 cells exposed to MDA CM shifted to higher values. (C-E) Single-cell analysis of speed/diffusivity/persistence. There were fold increases of 2.9, 5.1, 2.5 respectively on the speed, diffusivity, persistence of U937 cells exposed to MDA CM compared to control group U937 cells. (n=100. *P<0.05, **P<0.01, ***P<0.001, ****P<0.0005).

To consolidate this phenomenon, 3 biological repeats were carried out. Although the absolute values of single-cell speed/diffusivity/persistence were different each time, the overall trend of increased migration with MDA-MB-231 CM remained unchanged. Tumor associated macrophage infiltration in tumor bulk requires recruitment of monocytes and their migration towards tumor center. The increased migration of U937 monocytes after exposed to soluble factors secreted by MDA-MB-231 breast cancer cells indicates a paracrine pathway inside tumor niche to promote TAM infiltration.

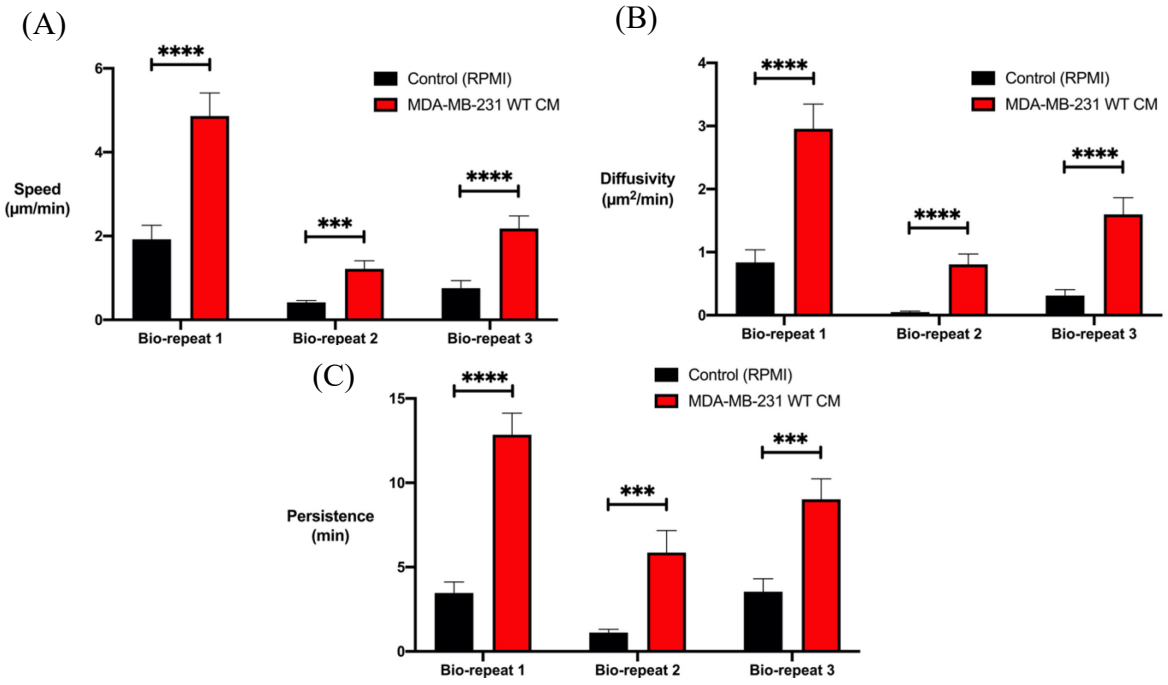

Figure 10: Summary of 3 biological repeats on U937 cells' increased migrations. (A-C) Across all 3 biological repeats, there were significant differences between MDA CM group and control group in terms of single-cell speed, diffusivity and persistence.

2.1.2 Conditioned media from TNBC and Melanoma increases primary monocyte migration

Considering of U937's lymphoma origin may to some extent change its physiological characteristics and cell properties as monocyte, for the following part of the study, primary monocytes isolated out from human peripheral blood are used. Classical $CD14^+$ primary monocytes were isolated via negative selection in order to leave the surface markers and activation status untouched during the isolation process. Same 3D cell migration experiment with MDA-MB-231 CM was carried out on primary monocytes with the addition of another CM from A375 melanoma cell line.

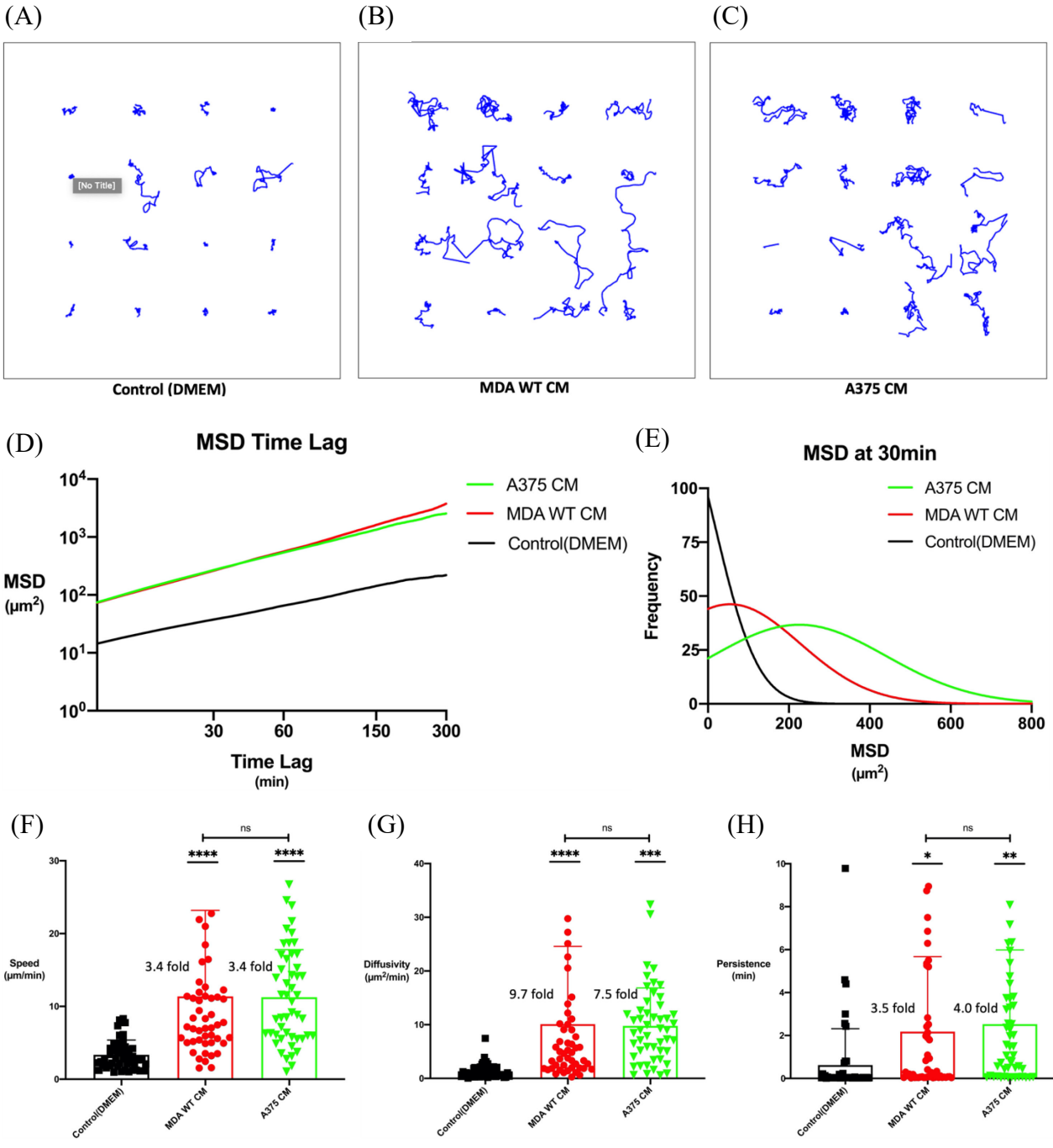

Figure 11: Trajectories, MSD distribution and single-cell analysis of primary monocytes exposed to MDA CM & A375 CM. (A-C) Random plotting of trajectories of primary monocytes exposed to fresh DMEM, MDA CM and A375 CM. More cell movements were shown in MDA CM and A375 CM groups. (D-E) Non-linear regression of MSD. MSDs of primary monocytes exposed to MDA CM & A375 CM shifted to higher values. A375 CM group showed more increases. (F-H) Single-cell analysis showed significant increases of speed/diffusivity/persistence for primary monocytes exposed to MDA CM & A375 CM compared to control group. While MDA CM group and A375 CM group showed no significant difference and had similar fold changes against control group. (n=50. *P<0.05, **P<0.01, ***P<0.001, ****P<0.0005).

From figure 11, we can see that primary monocytes were showing the same increased migration behavior as U937 cells when exposed to MDA-MB-231 CM. Interestingly, CM from melanoma A375 cell line seemed to exert same influence on primary monocytes. One possible explanation might be that both the MDA-MB-231 and A375 are hot tumor cell lines. Hot tumors, by definition, are solid tumors with massive number of T cell and macrophage infiltrations. Monocyte migration towards tumor center and invasive margin is the prerequisite for macrophage infiltration and consequently the increased migration of monocytes should in theory be observed for all hot tumor CMs.

2.2 IL6 accounts for increased monocyte migration

2.2.1 IL6 (not IL8) accounts for increased monocyte migration

As has previously mentioned in the introduction, there exists an IL6/IL8 synergistic autocrine pathway controlling density-dependent MDA-MB-231 migration in 3D collagen gel. Malignant growth of primary tumor results in extremely high cell density inside tumor bulk and thus creating an IL6/IL8-rich niche to promote tumor cell migration. Taking monocytes in tumor stroma also in consideration, we may come up with a hypothesis that this autocrine IL6/IL8 pathway of MDA-MB-231 cells can be the cause of increased migration for monocytes via a paracrine pathway since the JAK2/STAT3 cascade initiated by IL6/IL8 is essential for cell protrusion generation in 3D gel.

To verify this hypothesis, IL6 receptor and IL8 receptor expressions on the surfaces of primary monocytes were measured through flow cytometry. Based on figure 12, IL6R is highly expressed while IL8R shows low expression level.

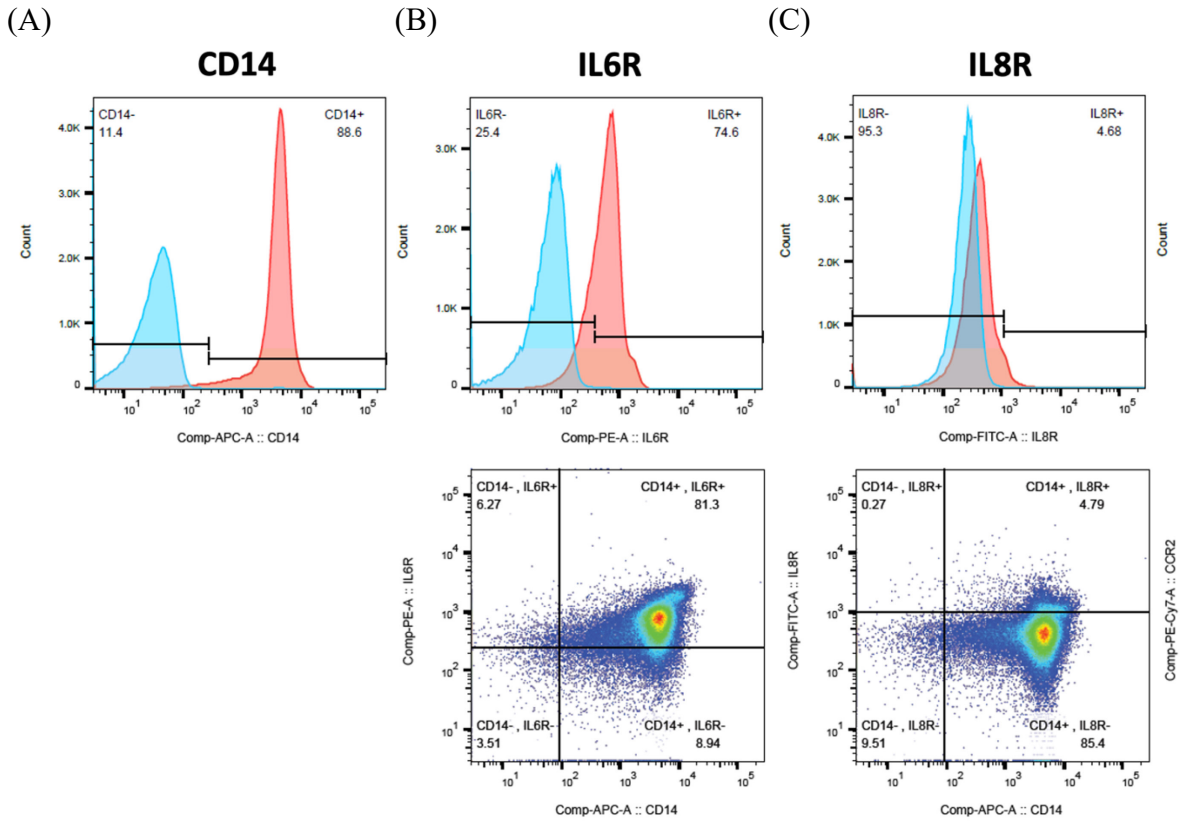

Figure 12: IL6R/IL8R expressions on the surfaces of primary monocytes. Blue curves represent isotype control results, red curves represent antibody binding results. (A) CD14 expression after isolation. CD14 is a pan-monocyte/macrophage marker for human primary monocytes. 88.6% of cells after PBMC isolation were primary monocytes. (B) IL6R expression on the surfaces of primary monocytes. 81.3% of primary monocytes were $CD14^{+}IL6R^{+}$. (C) IL8R expression on the surfaces of primary monocytes. 85.4% of primary monocytes were $CD14^{+}IL8R^{-}$.

Recombinant IL6 and IL8 were then added to fresh DMEM media to check if this could reproduce the phenomenon of increased monocyte migration induced by MDA CM. 300pg/mL was chosen as the concentration according to the density-dependent expression curve of IL6 and IL8 studied by Hasini Jayatilaka *et al.* In figure 13, MDA CM, IL6+IL8 and IL6 alone groups showed increased monocyte migration in terms of trajectories, MSD distribution and single-cell analysis. Surprisingly, there was no significant difference between IL6 alone group and MDA CM group, indicating that the mere IL6 molecule completely reproduced MDA CM's increased monocyte migration effect. IL8 alone group, in the other hand, showed no significant difference

compared with control group. Together with IL8R's low expression level on the surfaces of primary monocytes, it seems like it is IL6 in the MDA-MB-231 CM not IL8 that accounts for increased monocyte migration.

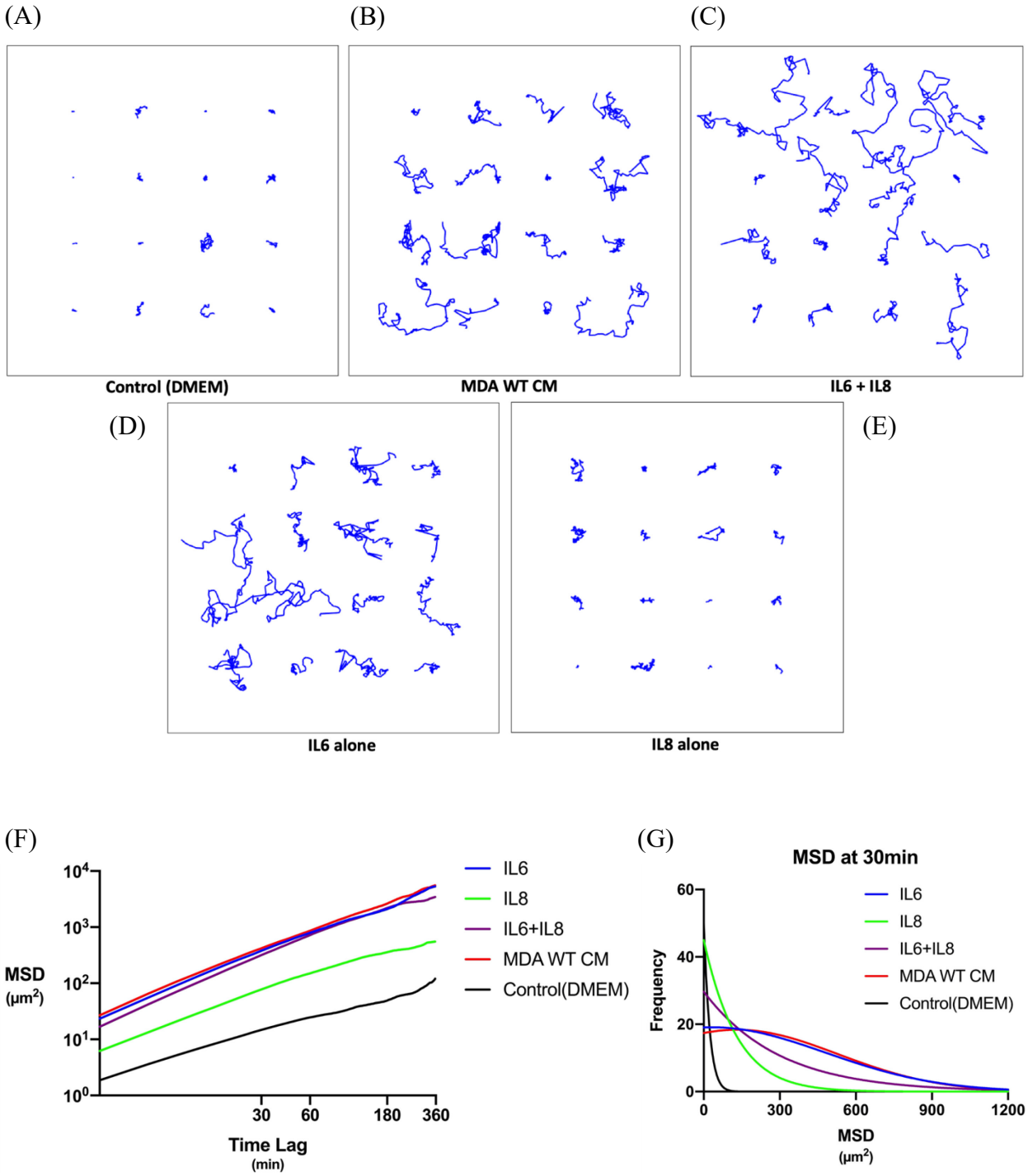

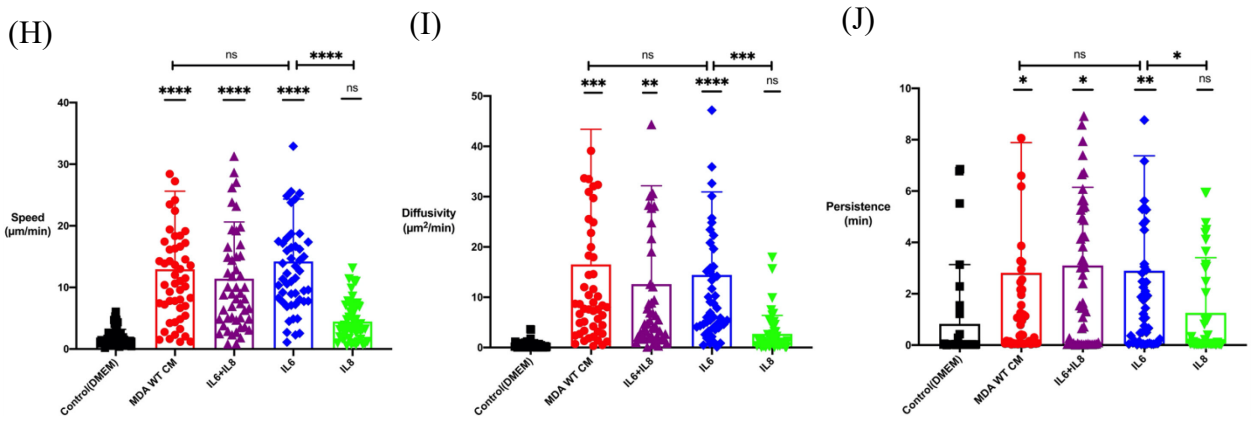

Figure 13: Trajectories, MSD distribution and single-cell analysis of primary monocytes exposed to MDA CM & IL6 & IL8. (A-E) Random plotting of trajectories of primary monocytes exposed to fresh DMEM, MDA CM, IL6+IL8 (300 pg/mL each) in DMEM, IL6 alone (300 pg/mL) in DMEM and IL8 alone (300 pg/mL) in DMEM. More cell movements were shown in MDA CM, IL6+IL8 and IL6 alone groups. (F-G) Non-linear regression of MSD. MSDs of primary monocytes exposed to MDA CM, IL6+IL8 and IL6 alone in DMEM shifted to higher values. MDA CM group curve and IL6 alone group curve overlapped. (H-J) Single-cell analysis showed significant increases of speed/diffusivity/persistence for primary monocytes exposed to MDA CM, IL6+IL8 and IL6. MDA CM, IL6+IL8 and IL6 alone groups showed no significant differences among each other and were all significantly increased compared with IL8 alone and control groups. (n=50. *P<0.05, **P<0.01, ***P<0.001, ****P<0.0005).

2.2.2 IL6R blocking inhibits increased monocyte migration

Tocilizumab is a drug already approved by FDA to block inflammatory cytokine IL6. Tocilizumab is able to competitively bind with IL6Rs on the surfaces of primary monocytes with high affinity and thus blocking interaction between IL6R and secreted IL6 in MDA CM. To verify if blocking of IL6Rs on primary monocytes can reverse their increased migration after exposed to MDA CM, tocilizumab was added in MDA CM and fresh DMEM with IL6. Based on figure 14, tocilizumab inhibited MDA CM and IL6's migration increasing effects on primary monocytes as we expected, making it a potential immunotherapy for mitigating monocyte and macrophage infiltrations into tumor center and invasive margin. However, there seemed to exist some remaining increased monocyte migration effects even though tocilizumab was added in MDA CM, indicating a more complex network of IL6 and other responsible soluble factors.

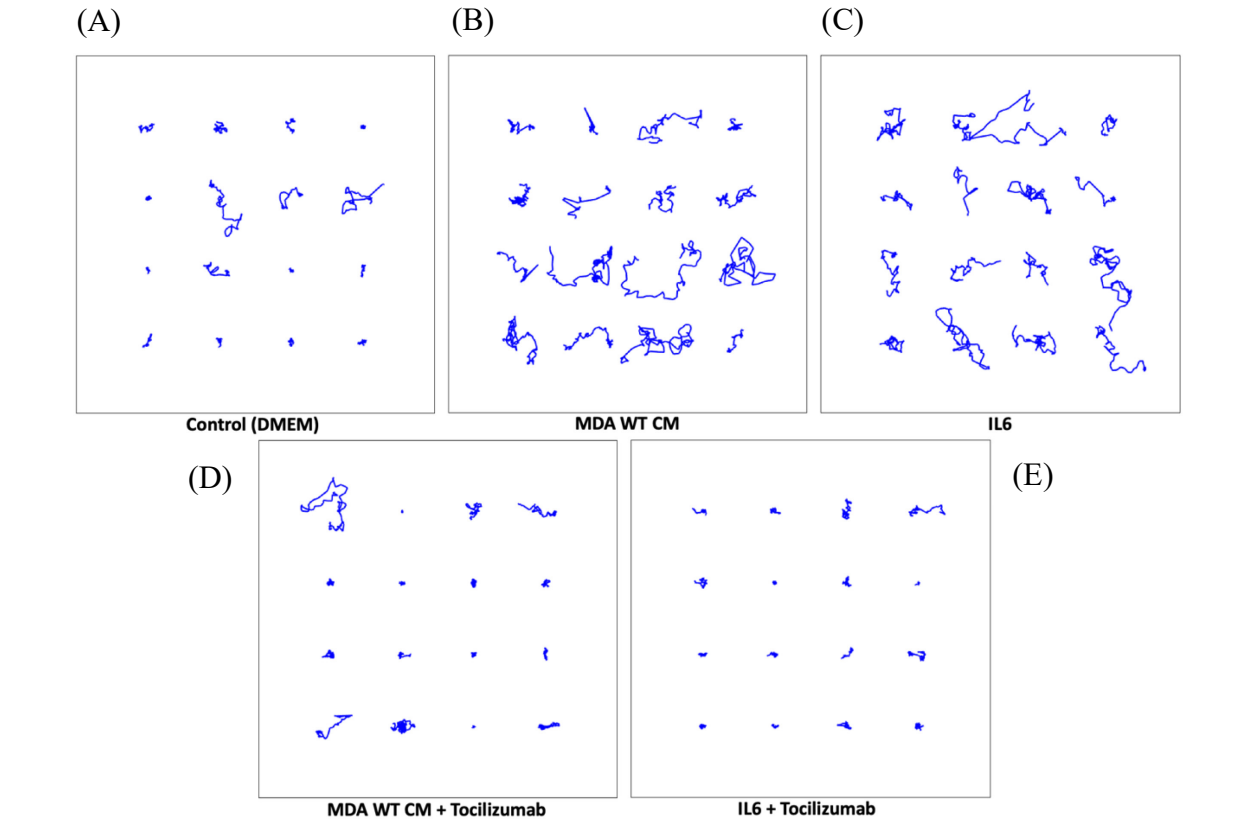
(A)
(B)
(C)
Control (DMEM)
MDA WT CM
IL6
(D)
(E)
MDA WT CM + Tocilizumab
IL6 + Tocilizumab

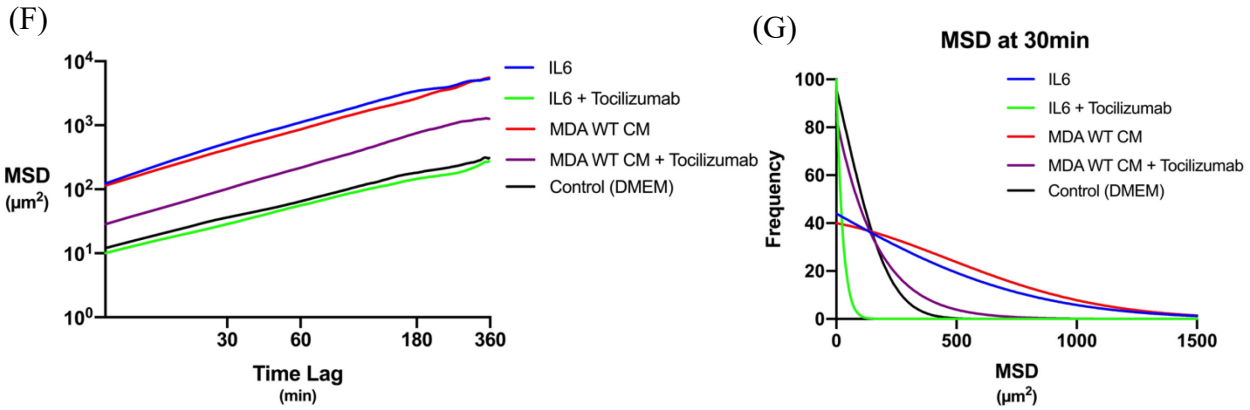
(F)
MSD (μm²)
Time Lag (min)
IL6
IL6 + Tocilizumab
MDA WT CM
MDA WT CM + Tocilizumab
Control (DMEM)
(G)
MSD at 30min
Frequency
MSD (μm²)

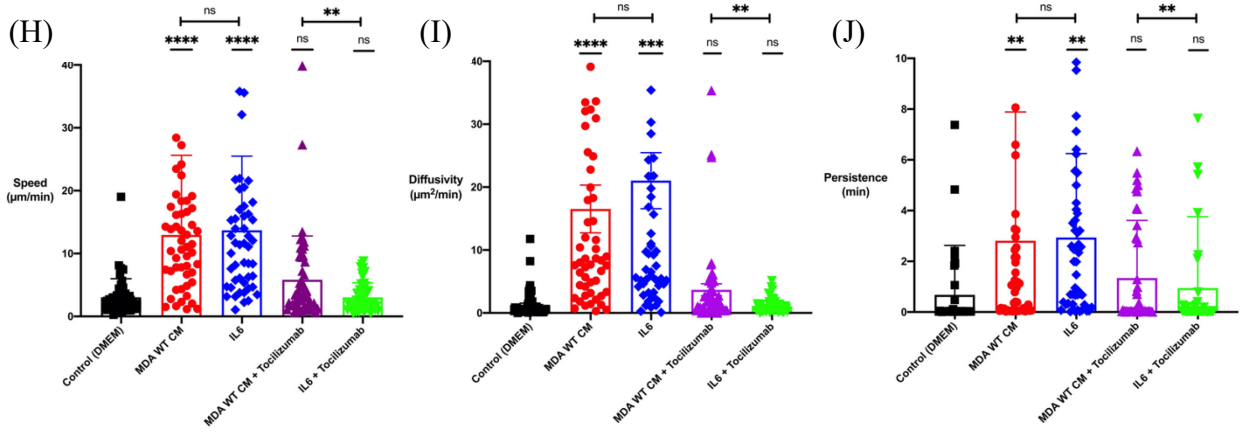
(H)
Speed (μm/min)
(I)
Diffusivity (μm²/min)
(J)
Persistence (min)
Control (DMEM)
MDA WT CM
IL6
MDA WT CM + Tocilizumab
IL6 + Tocilizumab

Figure 14: Trajectories, MSD distribution and single-cell analysis of primary monocytes with IL6R blocking using tocilizumab. (A-E) Random plotting of trajectories of primary monocytes exposed to fresh DMEM, MDA CM, IL6 (300 pg/mL) in DMEM, MDA CM+Tocilizumab (300ng/mL) in DMEM and IL6+ Tocilizumab (300 pg/mL IL6, 300ng/mL Tocilizumab) in DMEM. More cell movements were shown in MDA CM and IL6 groups. (F-G) Non-linear regression of MSD. MSDs of primary monocytes exposed to MDA CM and IL6 in DMEM shifted to higher values. MDA CM+Tocilizumab group curve and control group curve overlapped to some extents. (H-J) Single-cell analysis showed no significant increases of speed/diffusivity/persistence for primary monocytes after tocilizumab blocking. MDA CM and IL6 groups showed significant difference compared with tocilizumab blocking groups. (n=50. *P<0.05, **P<0.01, ***P<0.001, ****P<0.0005).

2.3 Enhanced migration & biased migration of monocytes

2.3.1 Definition of enhanced migration & biased migration

Increased migration mentioned before reflects on more cell movements in trajectories, MSD shifting to higher value and increased single-cell speed/diffusivity/persistence. All these migration behaviors are limited to cell random walk in 3D collagen gel. Here we bring in a new terminology as “enhanced migration” to describe faster random migration of cells. In contrast, chemotaxis, namely the directional migration of cells towards a chemoattractant source, can be concluded as “biased migration”, meaning more polarized migration. Enhanced migration and biased migration can be separated as two individual patterns for cell migration. To more vividly illustrate, cell migration resembles car driving, during which enhanced migration is the engine, controlling the moving speed while biased migration is the steering wheel, controlling the moving direction.

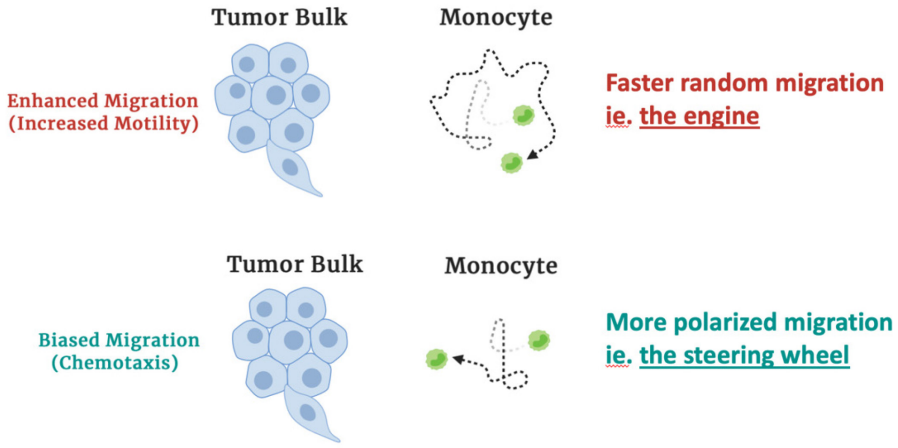

Figure 15: Definition of enhanced migration and biased migration. Monocytes with enhanced migration near tumor bulk are moving faster but randomly while monocytes with biased migration (chemotaxis) near tumor bulk are attracted towards tumor but move in normal speed.

2.3.2 Distinguish enhanced migration & biased migration

Chemotaxis of monocytes has long been studied and CCL2 (also called monocyte chemoattractant protein 1, MCP1) is identified as the most important chemokine for monocytes. In figure 16, we verified high expression of CCR2 (receptor of CCL2) on the surfaces of primary monocytes together with IL6R that is responsible for their enhanced migration.

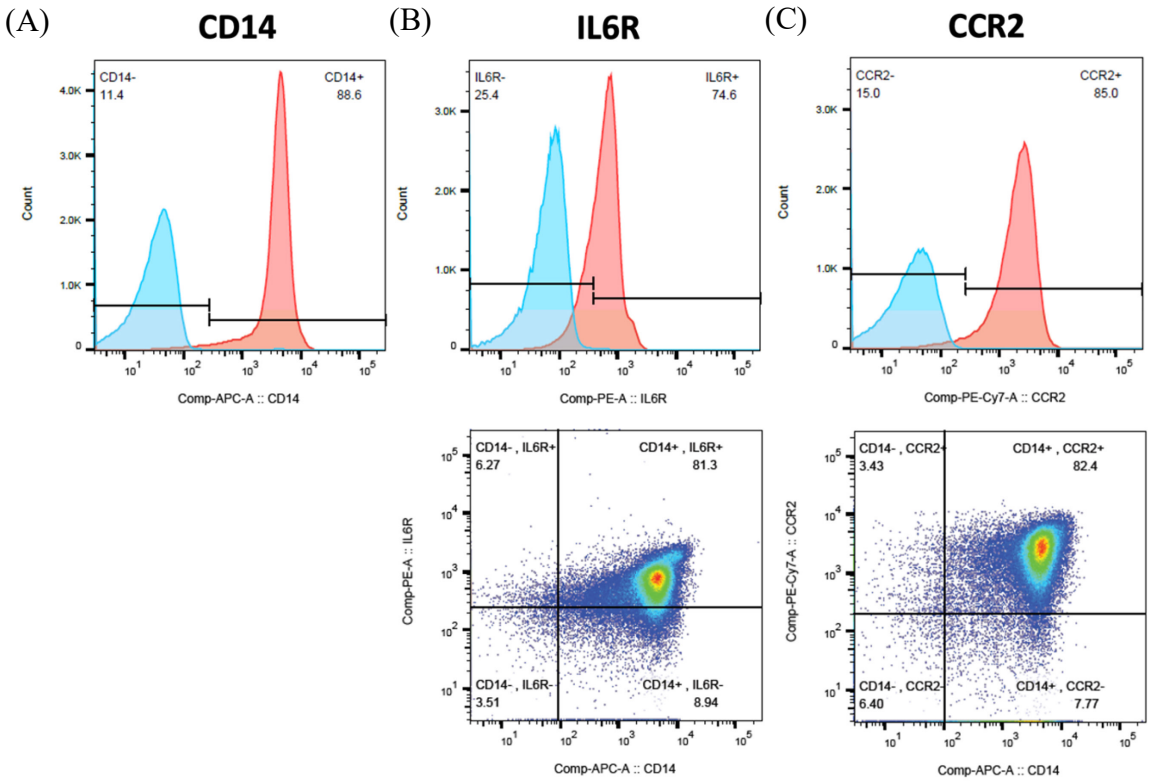

Figure 16: IL6R/CCR2 expressions on the surfaces of primary monocytes. Blue curves represent isotype control results, red curves represent antibody binding results. (A) CD14 expression after isolation. CD14 is a pan-monocyte/macrophage marker for human primary monocytes. 88.6% of cells after PBMC isolation were primary monocytes. (B) IL6R expression on the surfaces of primary monocytes. 81.3% of primary monocytes were $CD14^{+}IL6R^{+}$. (C) CCR2 expression on the surfaces of primary monocytes. 82.4% of primary monocytes were $CD14^{+}CCR2^{+}$.

To distinguish between enhanced migration and biased migration, CCL2 was added to fresh DMEM just like IL6 and was applied on primary monocytes in collagen gel. As is shown in

figure 17, CCL2 failed to reproduce IL6's increased monocyte migration effect but instead barely showed any enhanced migration.

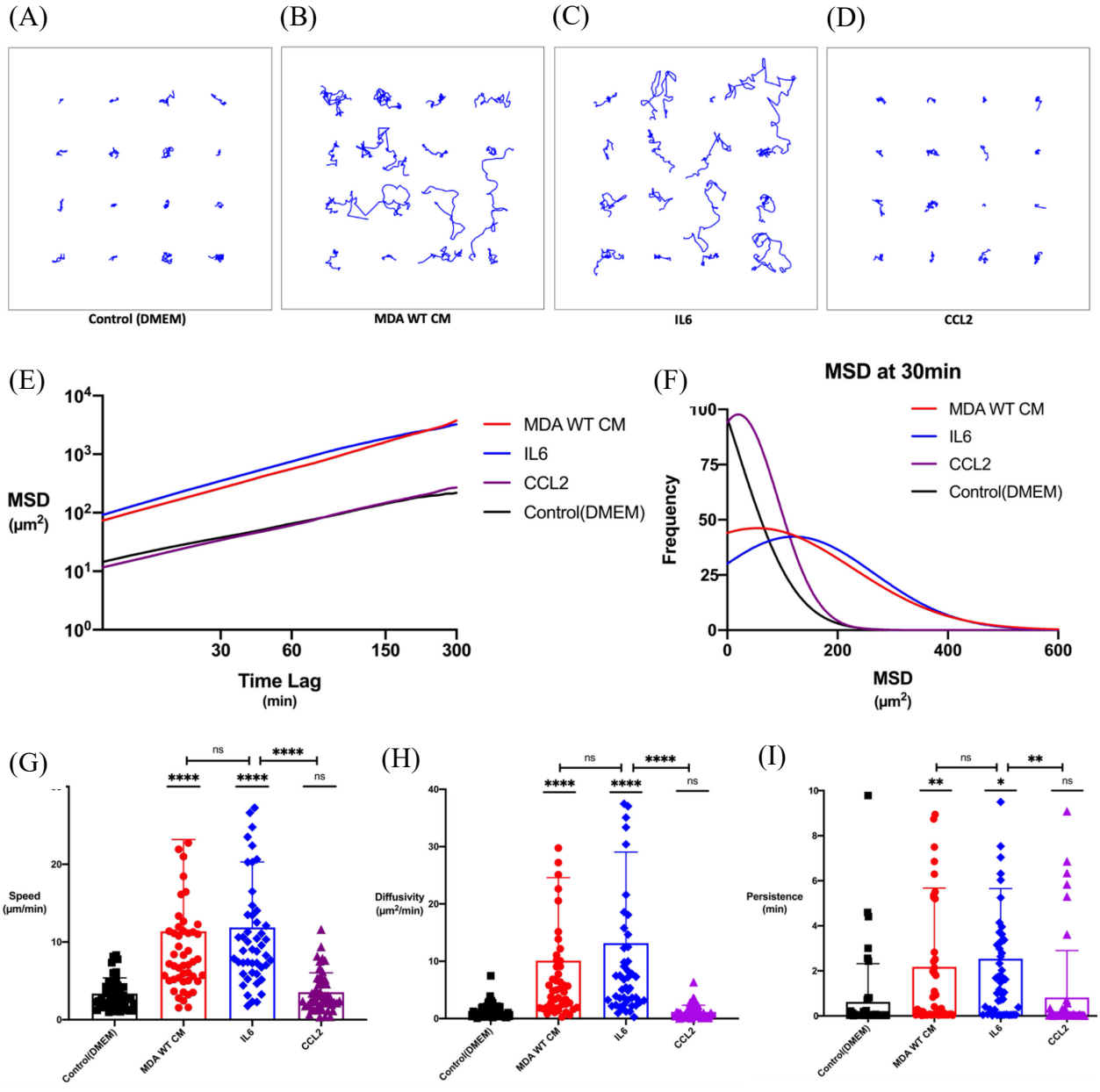

Figure 17: Trajectories, MSD distribution and single-cell analysis of primary monocytes exposed to chemokine CCL2. (A-D) Random plotting of trajectories of primary monocytes exposed to fresh DMEM, MDA CM, IL6 (300 pg/mL) in DMEM, CCL2 (300ng/mL) in DMEM. More cell movements were shown in MDA CM and IL6 groups. (E-F) Non-linear regression of MSD. MSDs of primary monocytes exposed to MDA CM and IL6 shifted to higher values. Both CCL2 group and control group had no cells over 200 μm^2 MSD at 30min. (G-I) Single-cell analysis showed no significant increases of speed/diffusivity/persistence for primary monocytes. MDA CM and IL6 groups showed significant difference compared with CCL2 and control groups. (n=50. *P<0.05, **P<0.01, ***P<0.001, ****P<0.0005).

From 3D cell migration study, we come into conclusion that CCL2 as a chemokine for biased migration has no effect on enhanced migration of primary monocytes. The next question to answer is whether IL6, as responsible soluble factor for enhanced migration, has influence on biased migration of primary monocytes. Simple transwell assay was carried out by seeding primary monocytes on top of the transwell insert membrane (5μm pore size) and added CCL2, IL6 and MDA CM in the bottom well as chemoattractant sources. After a 6-hour incubation, primary monocytes migrated down through membrane pores into the bottom well were viewed as undergoing chemotaxis. Based on figure 18, we can clearly see that MDA CM is capable of attract primary monocytes via biased migration like CCL2. IL6, on the other hand, was more comparable with DMEM control group in terms of cell numbers per unit area in the bottom well, showing no biased migration capability. In addition, using tocilizumab to block IL6Rs on the surfaces of primary monocytes had rare effect on their biased migration towards MDA CM, which further consolidates that IL6 for enhanced migration in MDA CM is not applicable to biased migration induced by CCL2. IL6 and CCL2 are mutually exclusive under their own mechanisms to affect monocyte migration. Putting together the 3D cell migration results and transwell results of IL6 and CCL2, the distinctive roles of enhanced migration and biased migration between monocyte and tumor cell interactions are confirmed.

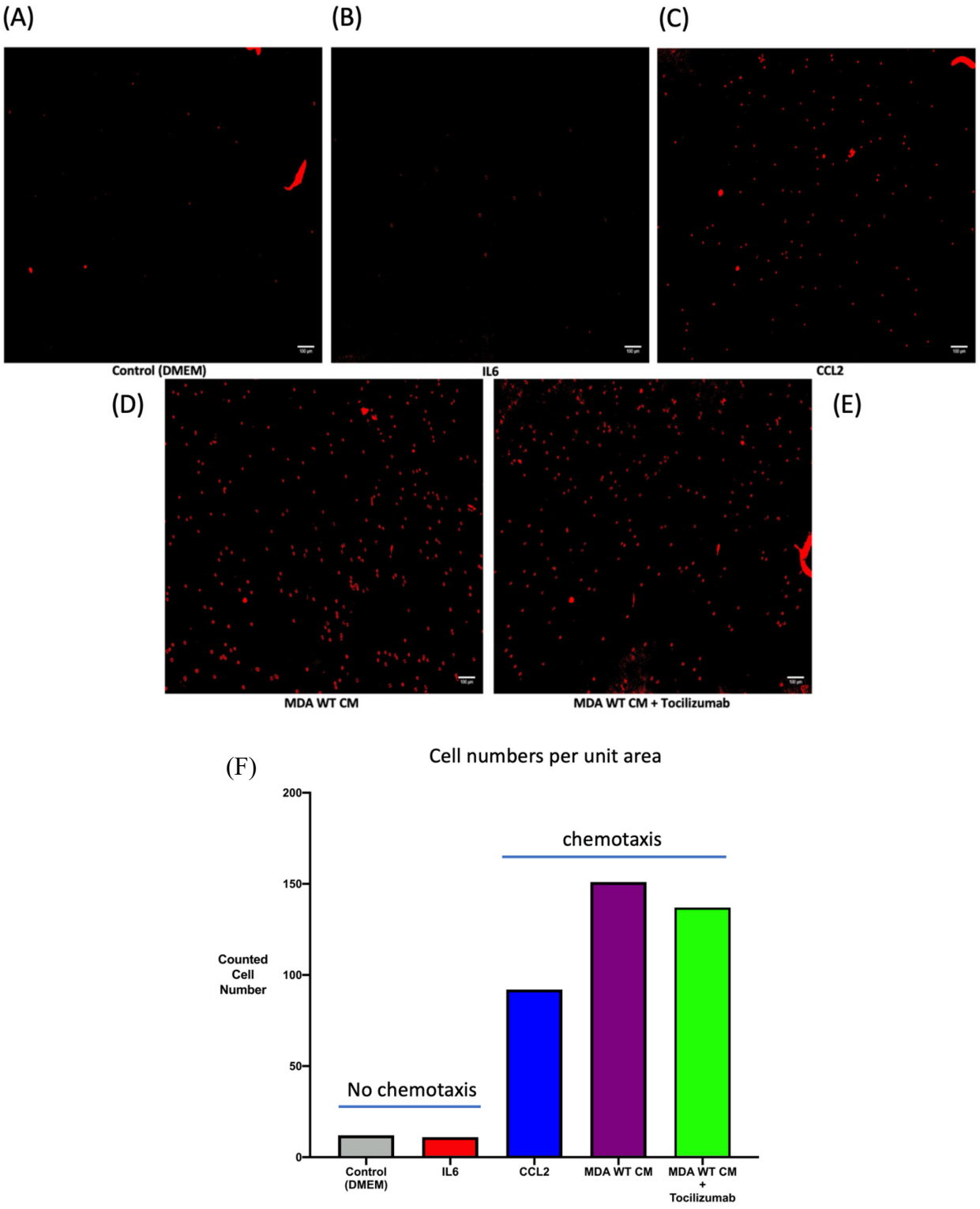

Figure 18: Pseudo-colored phase images of transwell assay and corresponding cell counting results. (A-E) Pseudo-colored phage images of different transwell conditions. There were more cells migrating into the bottom well when CCL2, MDA CM were applied. IL6R blocking using tocilizumab had no effect on MDA CM's chemo-attraction. (F) Counting results of cell numbers per unit area using imageJ particle analysis function. No chemotaxis happened for control and IL6 groups.

2.3.3 Combination of IL6-based enhanced migration & CCL2-based biased migration

From previous results we can learn that CM from MDA-MB-231 shows both IL6-dependent enhanced migration and CCL2-based biased migration effects on primary monocytes. Even distribution of soluble factors from tumor conditioned media into 3D collagen gel prevents the generation of chemoattractant gradients necessary for biased migration. To overcome this limitation, high density of MDA-MB-231 cells were embedded in pre-solidified matrigel cores to mimic solid tumor cores and later put into 3D collagen gel together with primary monocytes. As a result, with limited diffusion of soluble factors, primary monocytes initially located near MDA cores were exposed to both IL6 and CCL2 secreted by MDA cells while those initially located far away from MDA cores were supposed to work as control. In figure 19, 33 primary monocytes near one MDA core were tracked and trajectories showed a 2:1 ratio of monocytes moving towards the MDA core compared with those moving away from the MDA core, illustrating a biased migration pattern.

(A) (B)

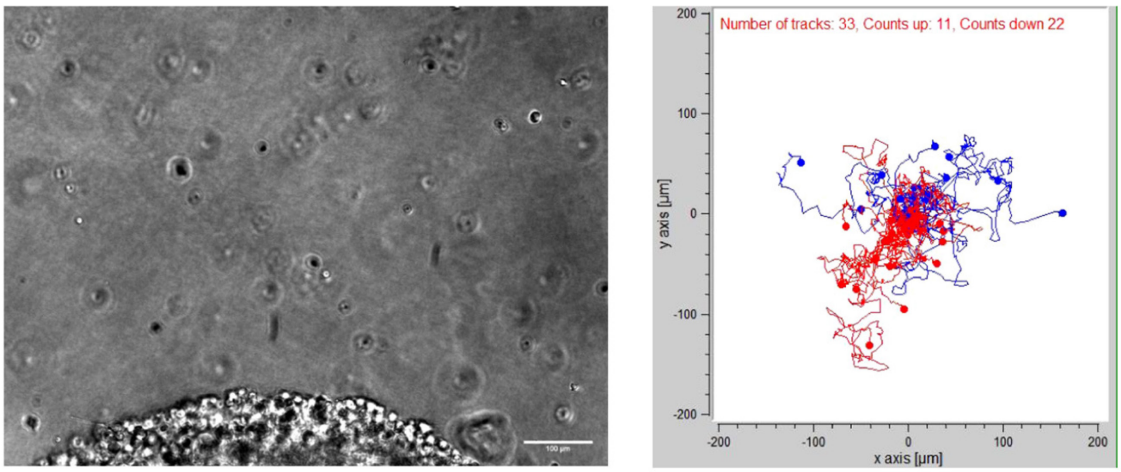

Figure 19: Biased migration of primary monocytes near the MDA core. (A) A 10x phase contrast image showing primary monocytes initially located near the MDA core. (B) Cell trajectories of 33 tracked primary monocytes near the MDA core. 22 monocytes (red trajectories) moving towards the MDA core (moving down) while 11 monocytes (blue trajectories) moving away from the MDA core (moving up).

In the meantime, by tracking all cells near the MDA core, figure 20 shows increased single-cell speed/diffusivity/persistence of monocytes near the MDA core compared with those away from the MDA core, illustrating an enhanced migration pattern.

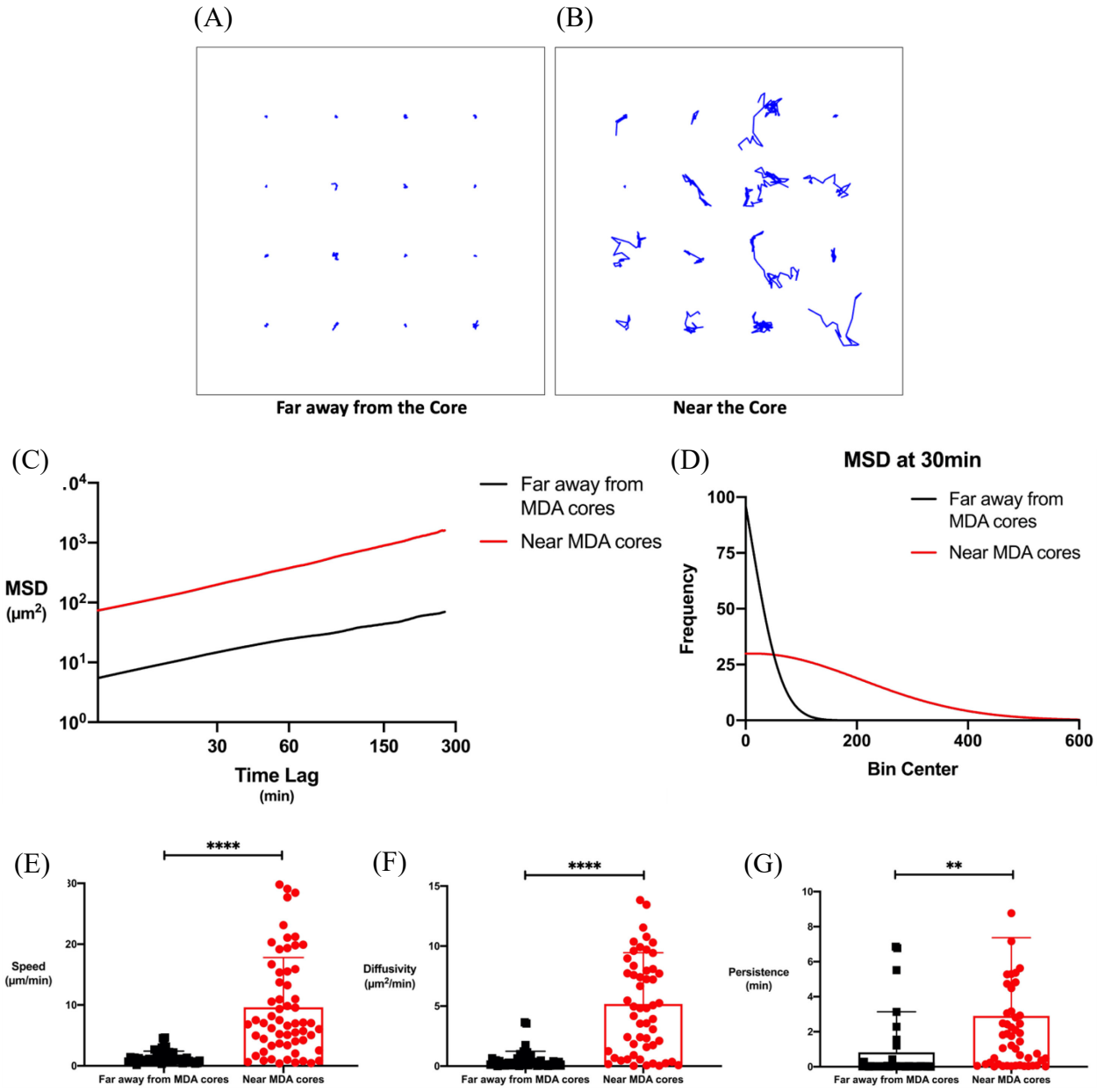

Figure 20: Trajectories, MSD distribution and single-cell analysis of primary monocytes near and away from MDA cores. (A-B) Random plotting of trajectories of primary monocytes near MDA cores and away from MDA cores. More cell movements were shown in monocytes near MDA cores. (C-D) Non-linear regression of MSD. MSDs of primary monocytes near MDA cores shifted to higher values. (E-G) Single-cell analysis showed significant increases of speed/diffusivity/persistence for primary monocytes near MDA cores. (n=50. *P<0.05, **P<0.01, ***P<0.001, ****P<0.0005).

To sum up, hot tumors (including triple negative breast cancer and melanoma) are able to increase monocytes' migration towards the tumor bulk via secreted soluble factors, during which an IL6-dependent enhanced migration and a CCL2-dependent biased migration work as a combination. Consequently, during monocytes' migration towards tumor center and invasive margin, these two separated migration patterns will work simultaneously to increase the overall recruitment of monocytes and lay the foundation for future re-education of monocytes into tumor associated macrophages.

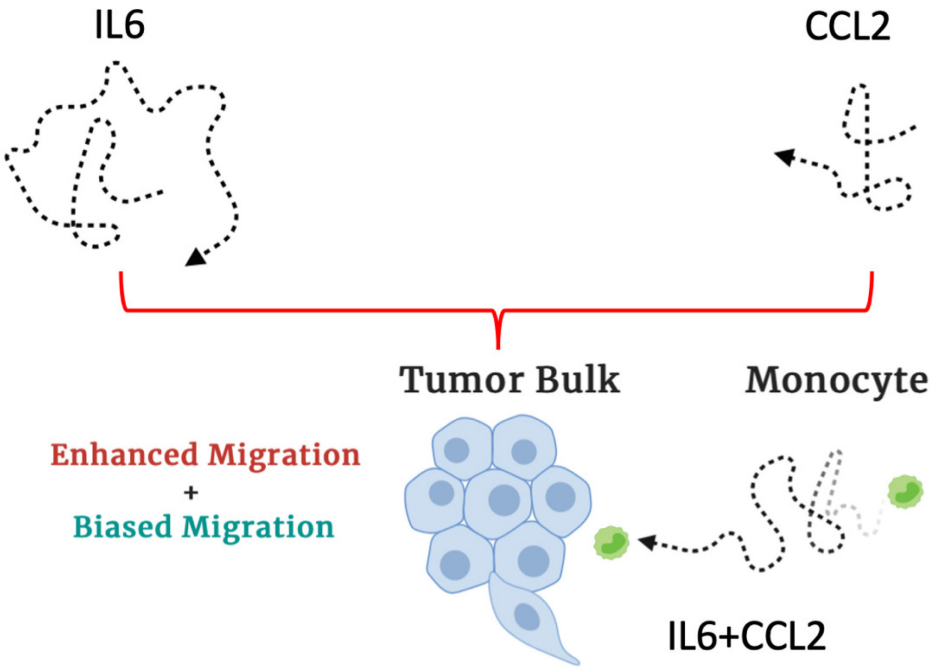

Figure 21: Combination of enhanced migration and biased migration during monocytes' migration towards tumor bulk. Tumor cells secrete IL6 and CCL2 and generate an IL6/CCL2-rich niche. Simultaneously, IL6 induces enhanced migration and CCL2 induces biased migration.

2.3.4 Loss of IL6R/CCR2 on the surfaces of macrophages

IL6R and CCR2 were shown to highly expressed on the surfaces of primary monocytes and are proved to be significant for enhanced and biased migration of monocytes in tumor

stroma ECM. Interestingly, after differentiating primary monocytes into M0 macrophages using M-CSF, all IL6R, IL8R and CCR2 were down-regulated as is shown in figure 22.

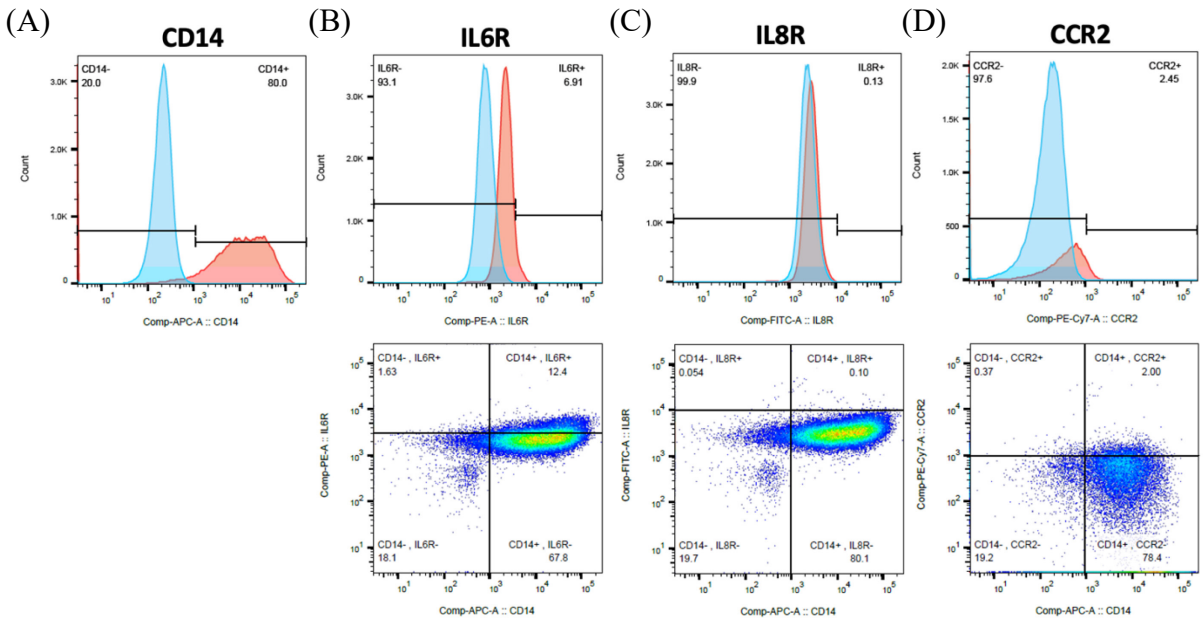

Figure 22: IL6R/IL8R/CCR2 expressions on the surfaces of primary macrophages. Blue curves represent isotype control results, red curves represent antibody binding results. (A) CD14 expression after isolation. CD14 is a pan-monocyte/macrophage marker for human primary monocytes. 80% of differentiated primary monocytes remained CD14 positive. (B) IL6R expression on the surfaces of primary monocytes. Only 12.4% of primary macrophages were $CD14^{+}IL6R^{+}$. (C) IL8R expression on the surfaces of primary monocytes. Only 0.1% of primary macrophages were $CD14^{+}IL8R^{+}$. (D) CCR2 expression on the surfaces of primary monocytes. Only 2% of primary macrophages were $CD14^{+}CCR2^{+}$.

People have long been confused on the order of monocyte recruitment and re-education. Whether monocytes get recruited and infiltrated into tumor bulk first and then get re-educated into tumor associated macrophages or the recruitment and re-education happen simultaneously remains an essential question to answer. Loss of IL6R and CCR2 on the surfaces of macrophages shown by flow cytometry data here indicates the loss of important migration abilities for macrophages, which indirectly support the statement that re-education happens after recruitment in that once monocytes are differentiated into macrophages, their migration capacities will get substantially mitigated.

2.4 TAMs promote cancer cell migration in 3D spheroid system

After solving the prerequisite question of how monocytes migrate towards tumor bulk, we will continue on digging into how these monocytes recruited in the vicinity of tumor center and invasive margin can get re-educated into tumor associated macrophages and in return promote tumor cell migration. A 3D double-layer co-culture spheroid system was adopted to overcome the limitation of widely used 2D wound-healing assay as a model for tumor cell migration.

2.4.1 Spheroid contraction rate is correlated with invasion of cancer cells

In a double layer 3D co-culture spheroid, a "basement" membrane composed of matrigel and a tumor stroma layer composed of type I collagen are provided to mimic the realistic tumor microenvironment. Highly metastatic MDA-MB-231 TNBC cells are embedded in matrigel core and can adopt a migratory phenotype to invade out into outer collagen layer, causing contraction of collagen. The entire spheroid provides a close contact microenvironment between tumor cells and monocytes, which resembles the stage after monocyte migration towards tumor bulk.

To clearly show the bio-distribution of monocytes inside spheroids, U937 cells were transduced with GFP-expressing lentiviral vectors and sorted.

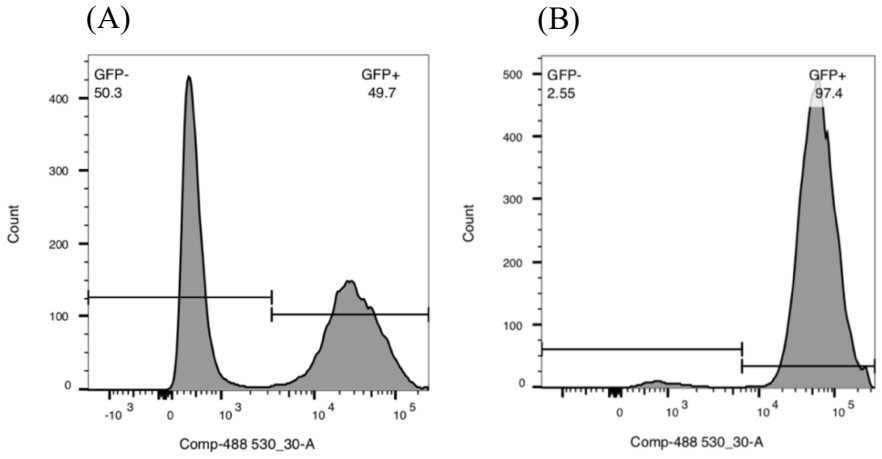

Figure 23: GFP expression on U937 cells after transduction and sorting. (A) Histogram of GFP expression after lentiviral transduction. 49.7% of U937 cells became GFP positive after successful transduction of lentivirus. (B) Histogram of GFP expression after cell sorting. 97.4% of U937 cells were GFP positive after sorting and culturing.

Different initial numbers of GFP^+ U937 cells were embedded into collagen layer surrounding the MDA tumor core in each spheroid. Volumes of spheroids were measured through phase contrast microscopy every day to show the contraction rates under different conditions. In addition, spheroids were harvested and sectioned in OCT compound for further invaded MDA-MB-231 cell counting. Illustrated by figure 24 (B-D), invaded MDA cell numbers were calculated out by subtracting total cell number (H33342 staining, DAPI channel) in the spheroid section with U937 cell number (FITC channel).

FITC images of spheroid sections showed rare infiltration of macrophages inside the MDA core. A positive correlation between spheroid contraction rates and invaded MDA cell numbers is shown in figure 24 (E-F).

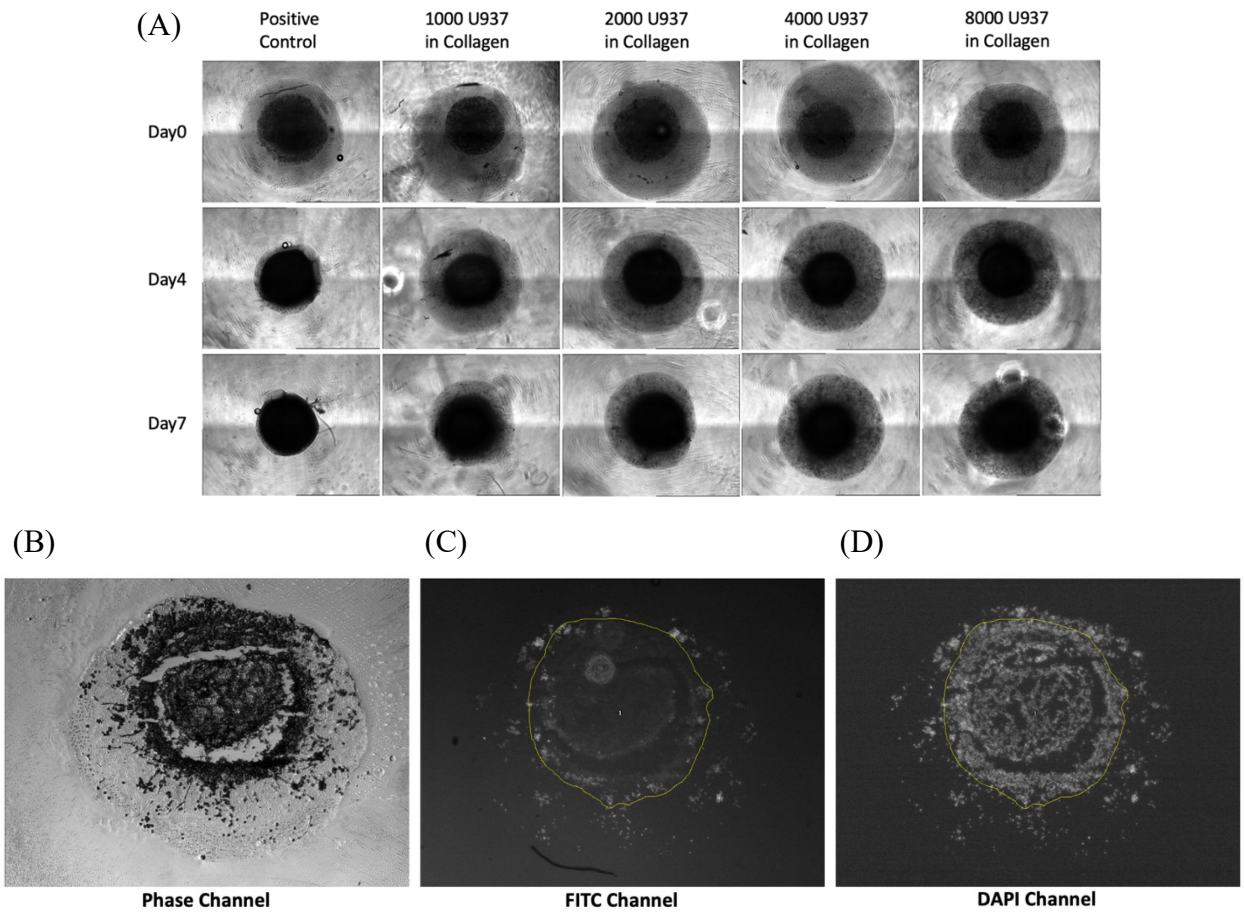

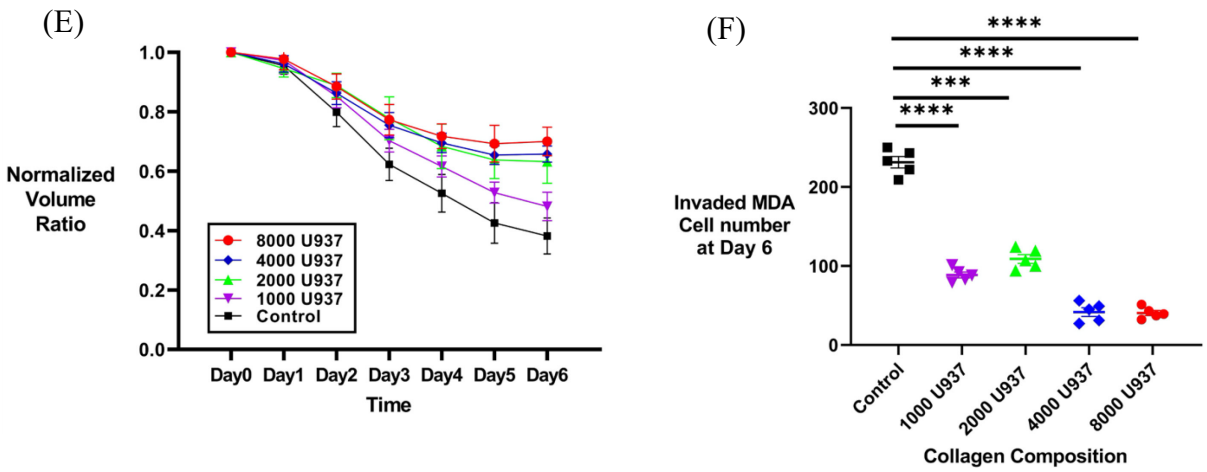

Figure 24: Spheroid contraction and invaded MDA cell counting in spheroid sections. (A) 4x stitched phase contrast images showing spheroids volumes on day0/day4/day7. Contraction of collagen was slower with more U937 cells initially embedded in collagen outer layer compared to control group with no U937 cells. (B-D) 4x phase contrast image, FITC channel image and DAPI channel image of a spheroid section. Cells with FITC signals were U937 cells while cells with DAPI signal were U937 and MDA cells together. MDA cells outside the yellow circle were considered as tumor cells invaded out into collagen layer. (E) Normalized spheroid volume ratios plotted against time. Volume of each spheroid on every day was normalized to its day0 initial volume to get a ratio value. Average of all spheroids under each condition was plotted (n=10 for each condition). (F) Invaded MDA cell numbers for different conditions. Subtraction of FITC channel cell number out from DAPI channel cell number gave out the invaded MDA cell number in each spheroid section (n=5 for each condition. *P<0.05, **P<0.01, ***P<0.001, ****P<0.0005).

2.4.2 Infiltration and re-education of tumor associated macrophages

To make more biological sense, primary monocytes were embedded into collagen outer layer of spheroids. Because primary monocytes are not transduced with GFP-expression lentivius, CD14-FITC conjugated antibody and CD206-Cy5 conjugated antibody were used for IHC staining of spheroid sections. CD14 staining would show the bio-distribution of primary monocytes/macrophages inside spheroids and CD206 (a widely used M2-like TAM marker) staining would show the re-education status of those primary monocytes. In figure 25, large amounts of FITC positive monocytes/macrophages were found infiltrated into the MDA core and the co-expression of CD206 verified the M2-like TAM nature of these infiltrated macrophages.

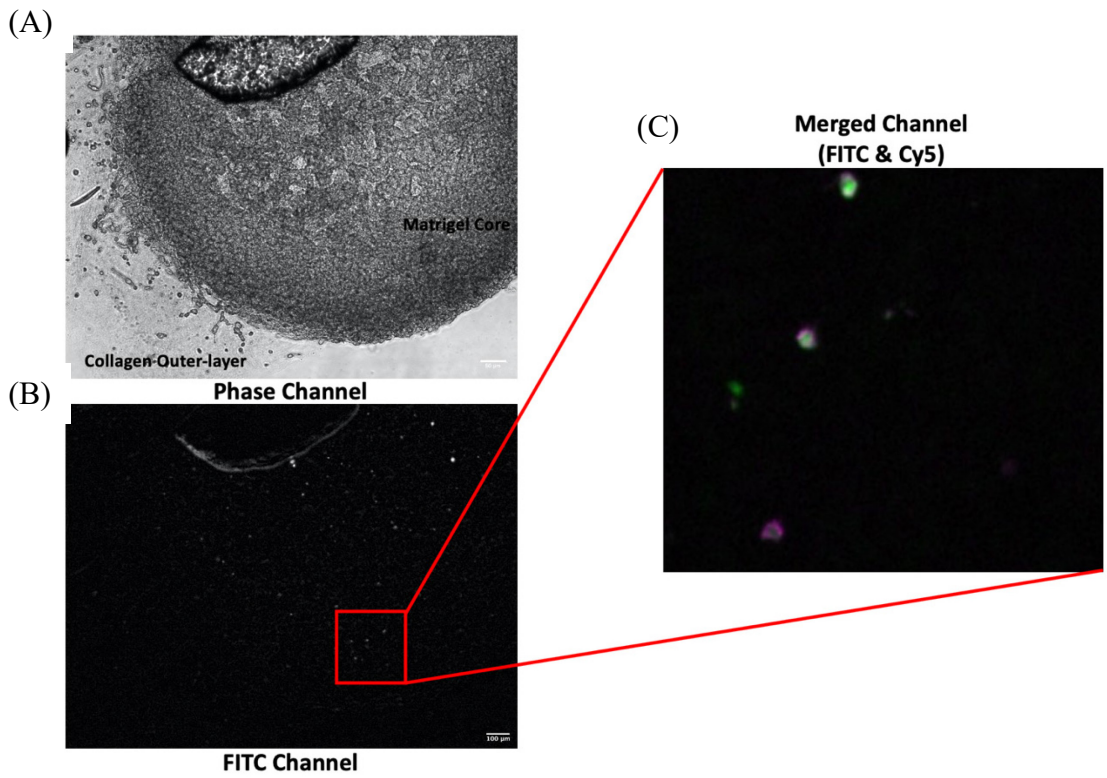

Figure 25: IHC staining of primary spheroid section. (A) 10x phase contrast image of a primary spheroid section. Darker part with higher cell density is the MDA core while lighter part is the collagen outer layer. (B) 10x FITC channel image of primary spheroid section. $CD14^+$ primary monocytes/macrophages were found located inside the MDA core. (C) Merged channel image of FITC(CD14) & Cy5(CD206). CD206 was co-expressed on $CD14^+$ primary macrophages.

2.4.3 Tumor associated macrophages promote cancer cell invasion

Contrary to the trend of U937 spheroids, contraction rates of primary monocyte spheroids were much faster compared to control spheroids with fresh media or polystyrene beads. As is shown in figure 26, the more primary monocytes were in the collagen, the faster the spheroid contraction was. Considering that a positive correlation of spheroid contraction rate and invaded MDA cell number has been established and these primary monocytes' re-educations into M2-like TAM phenotype, we can learn that tumor associated macrophages re-educated from monocytes in return promote MDA cell migration and invasion.

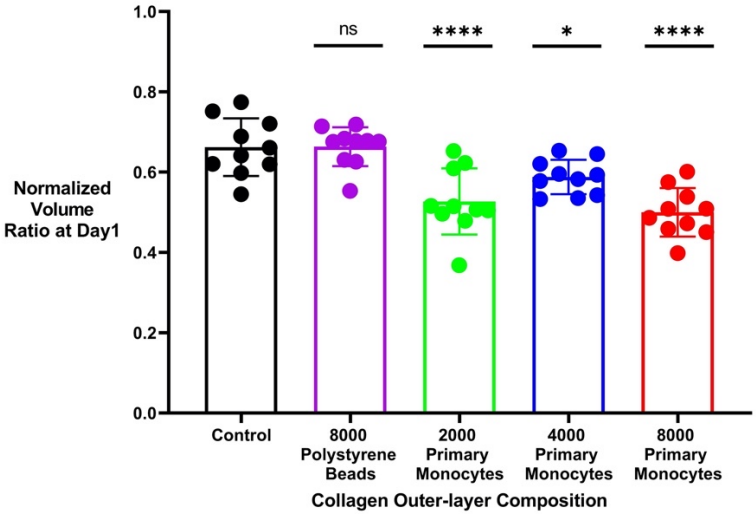

Figure 26: Normalized volume ratios of primary monocyte spheroids. Spheroids with primary monocytes embedded in collagen outer layer showed more reduction in volumes in contrast with spheroids with fresh DMEM and polystyrene beads.

Conditioned media from forced-educated M2 macrophages showed same tumor cell migration promoting effect in 3D collagen gel system. U937 cells were differentiated into M0 macrophages using PMA and then into M2 macrophages after stimulated with IL4/IL13. Figure 27 reiterates that M2-like tumor associated macrophages won't mitigate tumor cell migration compared with normal monocytes and naïve macrophages. No significant difference existed between U937 M2 CM group and the control group in terms of MDA single-cell speed/diffusivity/persistence. In comparison, after exposed to CM from U937 M0 macrophages and U937 monocytes, MDA cells underwent mitigated migration.

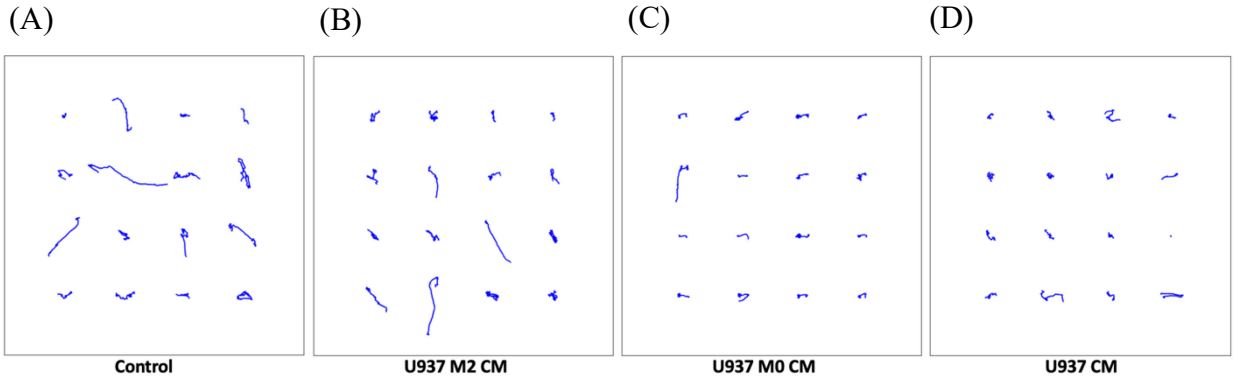

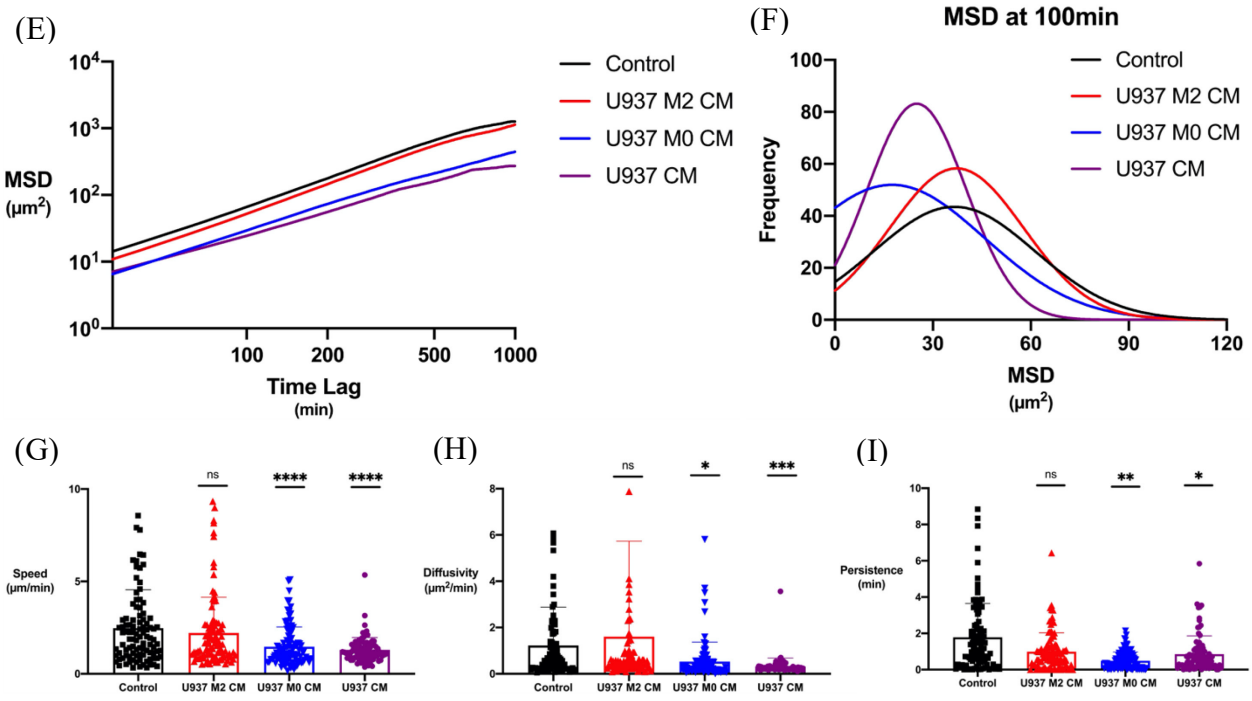

Figure 27: Trajectories, MSD distribution and single-cell analysis of MDA-MB-231 cells exposed to U937 monocyte CM and differentiated M0/M2 macrophage CM. (A-D) Random plotting of trajectories of MDA cells exposed to fresh DMEM, U937 M2 CM, U937 M0 CM and U937 CM. More cell movements were shown in control and U937 M2 CM groups. (E-F) Non-linear regression of MSD. MSDs of MDA cells exposed to fresh DMEM and U937 M2 CM shifted to higher values. (G-I) Single-cell analysis showed no significant decreases of speed/diffusivity/persistence for MDA cells exposed to U937 M2 CM. While U937 M0 CM and U937 CM groups showed significant decrease of speed/diffusivity/persistence compared with control group. (n=100. *P<0.05, **P<0.01, ***P<0.001, ****P<0.0005).

Re-education and pro-tumoral effects of tumor associated macrophages have long been heated topics in onco-immunology. Nevertheless, studies on TAMs are limited by lack of physiological-relevant 3D co-culture models. Under most circumstances, tumor conditioned media are harvested and applied on top of THP-1/U937 or human primary monocytes to examine soluble factors secreted by tumor cells that result in re-education of TAMs. To prove TAM's promoting effects on tumor invasion, simple 2D wound-healing assays on tumor cells are carried out using conditioned media derived from TAMs. Real cell migration in tissue ECM requires complicated combination of mechanisms including myosin contractility, actin assembly and microtubule-based polarization, which can only be properly explored using 3D ECM cell

migration models. In this study, a novel 3D two-layer co-culture spheroid system with matrigel and type I collagen was developed mimicking the real solid tumor basement membrane and stroma structure. A close interaction microenvironment for tumor cells and monocytes is provided and further analysis for TAM infiltration and re-education can be carried out via spheroid sectioning followed by IHC staining. In this study, primary monocytes were proven to be capable of infiltrating into TNBC tumor cores and in return promoting tumor cell migration after re-educated into tumor associated macrophages.

3. Methods and Materials

3.1 Cell culture

U937 monocytes (from ATCC) were cultured in RPMI 1640 (Gibco) supplemented with 10% (v/v) heat-deactivated FBS (Corning), 1% Penicillin-Streptomycin (Corning), 1% L-glutamine (Gibco) and 1% 1M HEPES buffer (Gibco). Human primary monocytes isolated out from PBMC were cultured in DMEM (Corning) supplemented with 10% heat-deactivated FBS (Corning) and 1% Penicillin-Streptomycin (Corning). MDA-MB-231 breast cancer cells and A375 melanoma cells were cultured in DMEM (Corning) supplemented with 10% FBS (Corning) and 1% Penicillin-Streptomycin (Corning). The cells were maintained in at 37°C and 5% CO_2 in a humidified incubator during cell culturing and during live-cell microscopy studies. FBS was considered to be successfully heat-deactivated after reaching 57°C in water bath and remaining for at least 30 minutes. All cells were passed after reaching 80% confluence in cell culture flasks.

3.2 Isolation of primary monocytes from PBMC

PBMC (Peripheral blood mononuclear cells) were prepared from leukopaks via standard Ficoll-Paque^{TM} PLUS (GE Healthcare) density-gradient-based isolation process. After Ficoll

isolation, PBMCs were frozen down in a density of $5*10^7$ cells/mL in freezing media (90% FBS, 10% RPMI 1640). Negative selection isolation of classical $CD14^+$ primary monocytes was carried out using Human Pan Monocyte Isolation Kit (Miltenyi Biotech). Protocol recommended was used for the isolation process. After isolation, flow cytometry was done to confirm CD14 expression on the surfaces of isolated cells. Later, primary $CD14^+$ monocytes were cultured or directly embedded into 3D collagen gel or spheroids for future use.

3.3 3D type I collagen ECM gel making for single-cell migration assay

Cell suspensions containing 50,000 cells in a 1:1 (v/v) ratio of cell culture media and reconstitution buffer (220mg sodium bicarbonate and 480mg of HEPES sodium salt resolved in 10mL of DI water and filtered with 0.22μm PVDF filter) were mixed with high concentration (8-9mg/mL) of rat-tail type I collagen (Corning) to obtain a final collagen concentration of 2mg/mL (for U937 cells) or 1mg/mL (for primary monocytes). The whole process of mixing was carried out on ice to prevent the solidification of collagen under room temperature. A calculated volume of 1M NaOH was quickly added into the mixture to tune the final pH around 7. 500L of cold cell-suspension gel mixture was then aliquoted into a 24-well flat-bottom cell culture dish on a plate heater set to 37°C for approximately 10 minutes and then transferred to incubator maintained at 37°C for 1 hour to allow for further polymerization and formation of collagen fibers. 500 μL of different conditioned media were added on top of solidified collagen gel followed by another 1-hour incubation at 37°C for even distribution of soluble factors. A overnight video was taken under 10x phase contrast microscope with live-cell box (37°C and 5% CO_2) with a time interval of 3 minutes. Five locations were randomly chosen in each well with focus set at the middle layer of gel.

3.4 Cell tracking using MetaMorph software

NIS Elements software was used to split the entire overnight video into separated videos at each location. ND2 video files were transformed into tiff video files using imageJ macros. Tiff video files were imported into MetaMorph software (version 7.0.0) for tracking. For videos at each location, 10 cells were randomly chosen as tracking objects and tracking information of all tracked cells under the same condition were combined together.

3.5 Single-cell analysis for cell migration

Anisotropic persistent random walk (APRW) model previously developed by Pei-Hsun Wu *et al* was applied for single-cell migration analysis in 3D collagen gel[18]. MATLAB codes were obtained from the corresponding Nature Protocols paper[19]. Cell tracking information from MetaMorph was input into MATLAB for trajectory generating, MSD calculating and speed/diffusivity/persistence calculation.

Figures of MSD and single-cell speed/diffusivity/persistence were generated in Graphpad using values output from MATLAB.

3.6 Lentivirus production and transduction

The bacteria stock of lentiviral vector (pHAGE NFkB-TA-LUC-UBC-GFP-W) was purchased from Addgene (plasmid#: 49343). Bacteria were inoculated on agar plates with ampicillin (100μg/mL). After overnight incubation at 37°C, single colonies were picked using 10uL microtips and transferred into 4mL of LB broth containing 100μg/mL ampicillin under sterile condition. Liquid cultures of bacteria were incubated overnight in shaker at 37°C and 220rpm/min. After transparent LB broth turned into turbid appearance, a miniprep was carried out using QIAprep Spin Miniprep kit (QIAGEN). Concentration of eluted lentiviral plasmids were detected using Nanodrop^{TM} 2000 spectrophotometer.

HEK-293T cells seeded in 10cm petri dish were co-transfected with three plasmids (GFP-expressing lentiviral vector, DR 8.91, and pCMV-VSVG) using the standard calcium phosphate precipitation protocol. After 24 hours, the media with remaining plasmids were swapped with fresh DMEM. 48h and 72h media containing lentivirus were harvested and combined, followed by a filtration using 0.45μm PVDF filter to remove cell debris. Filtered lentivirus media were stored under -80°C for future use.

Polybrene and spinoculation were adopted to boost the transduction efficiency for boosting the transduction efficiency of U937 cells. 10μg/mL of final concentration polybrene was added into lentivirus media (multiplicity of infection, MOI = 30) and applied on top of U937 cells. A standard 30-min spinoculation was carried out followed with additional 48h incubation under 37°C and 5% CO_2. After 48 hours, U937 cells were passed into fresh RPMI and let grow for one more generation.

Sony SH800 cell sorter was used for sorting out GFP^+ U937 cells. After sorting, GFP^+ U937 cells were kept in culture for further use.

3.7 3D double-layer co-culture spheroid making

For preparation, 10L of serum free DMEM and 45μL of mineral oil was added into non-filtered 10μL tip (oil layer floating on top of aqueous DMEM layer). Wild type MDA-MB-231 cells were trypsinized, pelleted, and re-suspended in ice-cold matrigel (Corning) such that the final concentration of cells was 80,000/μL. 1μL of cell-matrigel mixture was dropped into the oil layer of each 10μL tip and a spheroid-shape of matrigel core would be formed dur to surface tension. After a 1-hour incubation at 37°C for solidification, these matrigel cores were harvested using pre-cut 200μL tips and washed with fresh DMEM. For second collagen layer making, U937 or primary monocytes were embedded together with MDA-MB-231 matrigel cores inside collagen mixture to

make the final concentration as 2mg/mL (for U937 cells) or 1mg/mL (for primary monocytes). 5μL of this collagen mixture with one MDA-MB-231 matrigel core was taken with pre-cut 200μL tip and dropped into mineral oil layer like previously shown. After a 1-hour incubation at 37°C for solidification, these double-layer co-culture spheroids were harvested using pre-cut 200μL tips and washed with fresh DMEM for 3 times. One final spheroid together with 200μL of fresh DMEM was transferred to one well of a round-bottom 96-well plate. Due to gravity, spheroids would sink down to bottom centers of 96-well plates.

3.8 Quantification of spheroid volumes

Because a 4x phase contrast image can't cover the whole spheroid, 4 images covering 4 corners were taken together and later stitched together. Volume of spheroids were measured through measuring their diameters in NIS Elements software and calculating using the equation $V = \frac{4}{3}\pi R^3$.

3.9 Section of spheroids and IHC staining

Individual spheroids from same conditions were harvested and wasted with 1x DPBS (Gibco) for 3 times. After washing, spheroids were fixed under room temperature using 4% PFA for 20 minutes. Successful fixation was shown as all spheroids sink down to the bottom of Eppendorf tubes instead of floating. 3-4 spheroids were transferred into one cryomold (SAKURA Tissue-Tek, 10mm*10mm*5mm) using pre-cut 200μL tips. Syringes were used to suck out remaining PBS in the plastic mold and then OCT compound (SAKURA Tissue-Tek) was added inside to fill up the entire volume. Plastic mold with spheroids embedded in OCT compound were then quickly frozen down in liquid nitrogen until transparent OCT compound turned into milky white solid phase. All plastic molds were stored under -80°C for future use.

Sectioning was carried out using Cryostat Microm HM550 (Thermo Scientific). Each time one OCT compound cubic was mounted onto the cryostat mounting stand and then transferred into the sectioning chamber. Chamber temperature was set to -22°C and mounting temperature was set to -18°C in order to soften the OCT compound cubic for easier cutting. During sectioning process, trimming thickness was set to 10μm and section slices were attached on pre-polarized microslides (Thermo Scientific) for dehydrating and storage.

For following IHC staining, section slices were covered using glass coverslips. Rehydrate the section slices with 1x DPBS for 10 minutes. Block non-specific binding between primary antibodies and cells for 30 minutes under room temperature using blocking buffer (1% horse serum in PBS). Primary antibodies diluted in incubation buffer (1% bovine serum albumin, 1% horse serum, 0.3% Triton® X-100, and 0.01% sodium azide in PBS) were applied on section slices followed by a 4°C overnight incubation in fridge. After primary antibody staining, wash section slices with 1x DPBS for three times (15 minutes per time) and incubate with secondary antibodies diluted in incubation buffer for 1 hour under room temperature. The secondary antibody staining process was kept out from light due to their photo-sensitivities. Wash 3 times with 1x DPBS and mount section slices in fluorescence anti-fading mounting media (VECTOR, VECTASHIELD H-1000).

3.10 Flow cytometry

All flow cytometry antibodies were bought from BioLegend including FITC anti-human CD181 (IL8Ra), PE anti-human CD126 (IL6Ra), PE/Cy7 anti-human CD192 (CCR2) and APC anti-human CD14. Cells Fc receptors were blocked with FcX™ (BioLegend) for 15 minutes under room temperature. 30 minutes' incubation at 4°C was applied for antibody staining. Samples were run by BD Canto flow cytometer.

4. Supplementary figures and data

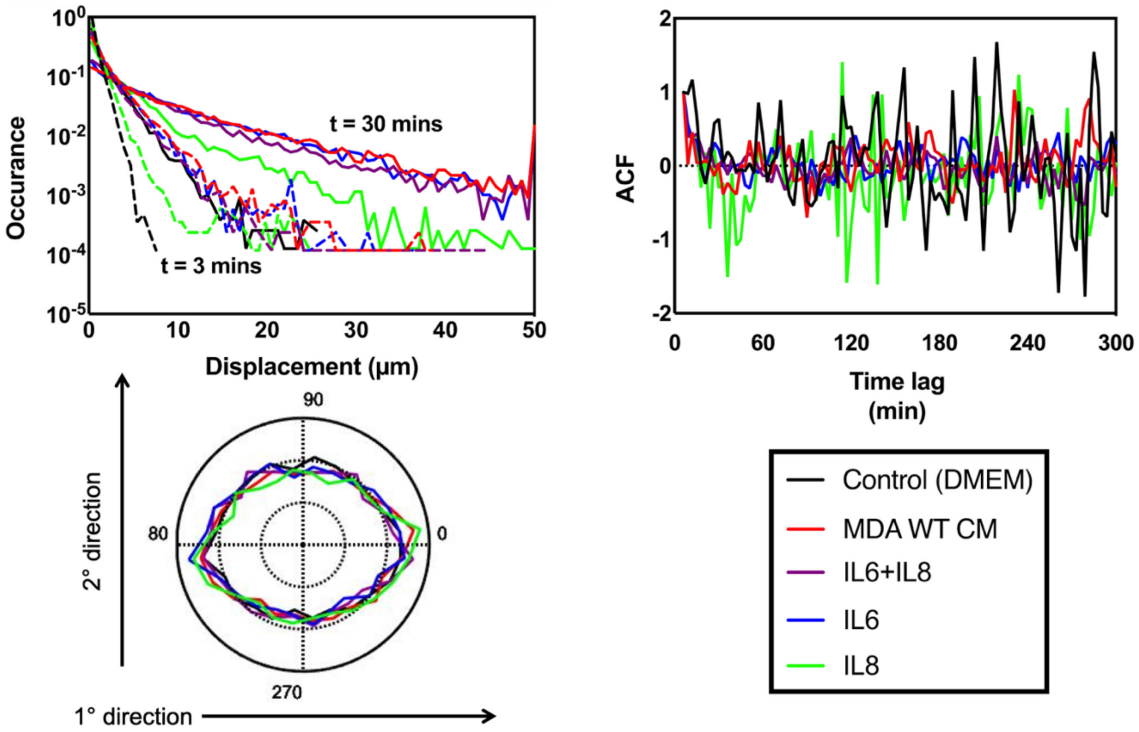

Figure S1: Displacement, auto correlation function (ACF) and angular velocity analysis on IL6/IL8 monocyte migration assay. In displacement figure, solid lines are cell displacement occurrence curves at frame 10 (30 mins) and dash lines are cell displacement occurrence curves at frame 1 (3 min). It is obvious that cells in MDA CM, IL6+IL8 and IL6 groups had higher occurrences of larger displacements.

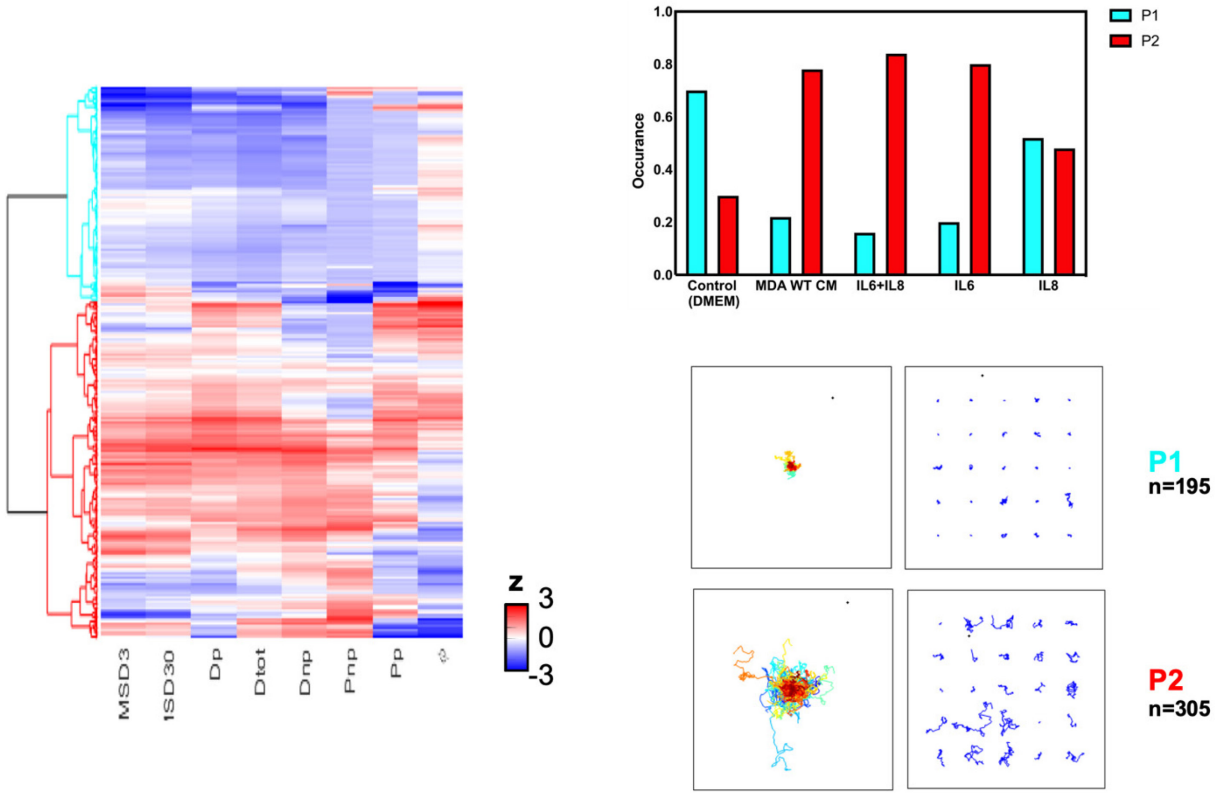

Figure S2: Spatial clustering of all tracked monocytes in IL6/IL8 migration assay. 8 parameters including MSD at 3min, MSD at 30min, Dp (diffusivity along primary axis of migration), Dnp (diffusivity along secondary axis of migration), Dtot (total diffusivity), Pp (persistence along primary axis of migration), Pnp (persistence along secondary axis of migration) and Psi (ϕ, anisotropy). Two cell population clusters were defined as P1 and P2. P2 represented cells with increased migration abilities. Similar to single-cell analysis results, MDA CM, IL6+IL8 and IL6 groups showed shifted distributions to higher-migration-ability cell populations compared to control and IL8 group.

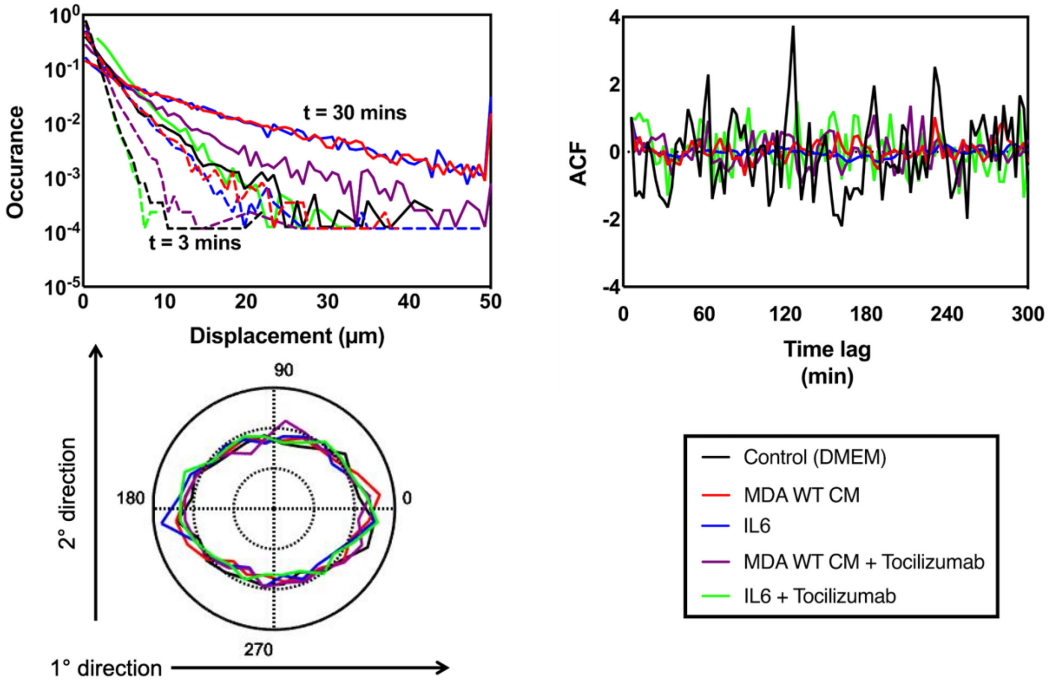

Figure S3: Displacement, auto correlation function (ACF) and angular velocity analysis on tocilizumab blocking monocyte migration assay.

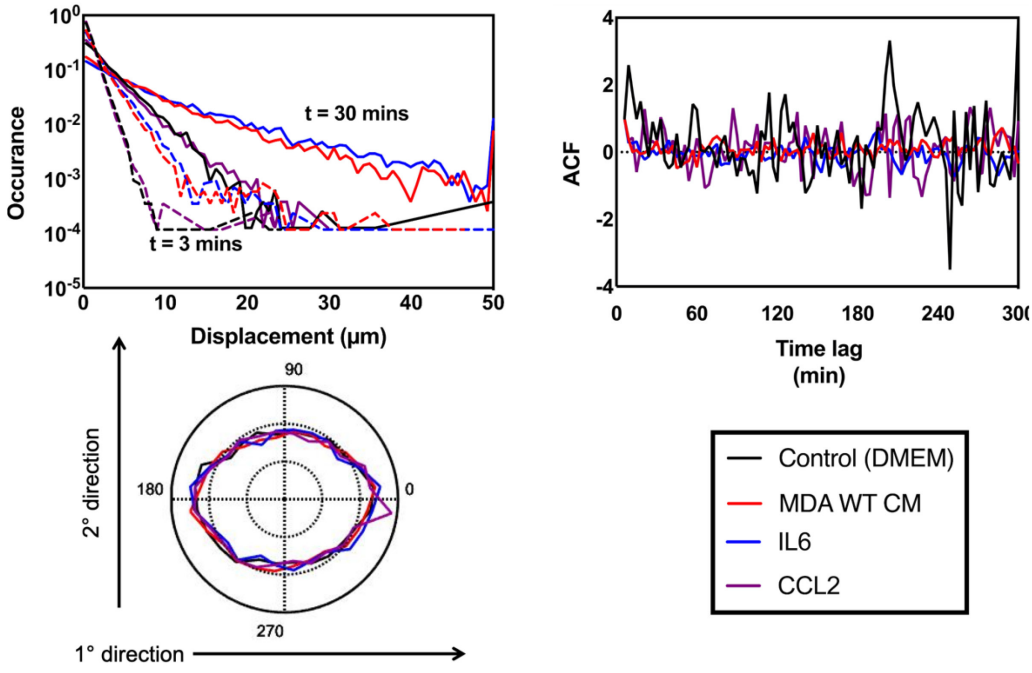

Figure S4: Displacement, auto correlation function (ACF) and angular velocity analysis on IL6/CCL2 cell migration assay.

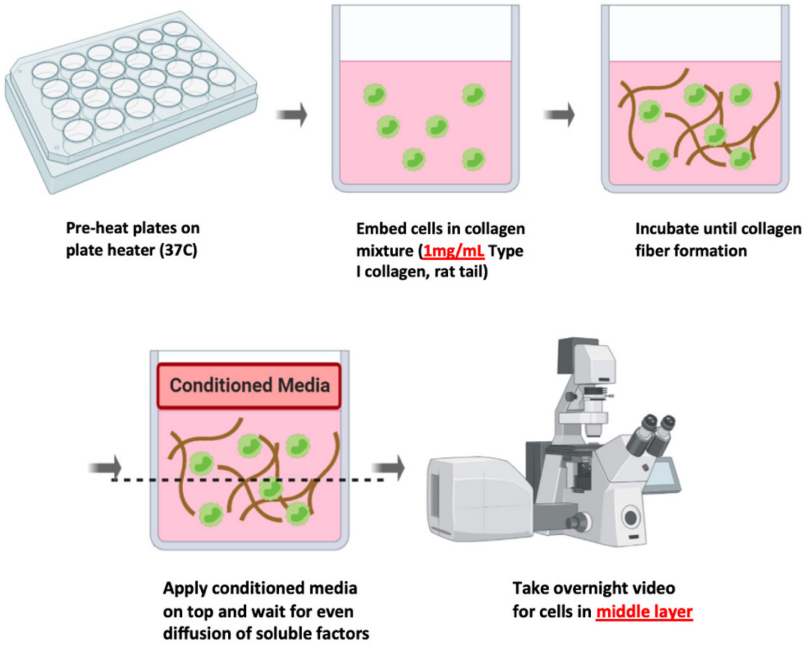

Figure S5: Scheme of 3D type I collagen gel making. 50,000 monocytes were embedded into 500μL collagen (2mg/mL or 1mg/mL). Conditioned media were put on top of already solidified collagen gel. Incubate for 1h until diffusion of soluble factors was even. Set up a 3-min-interval video taking procedure on microscope with live cell box. Analyze at least 120 frames of videos for single cell speed/persistence calculation.

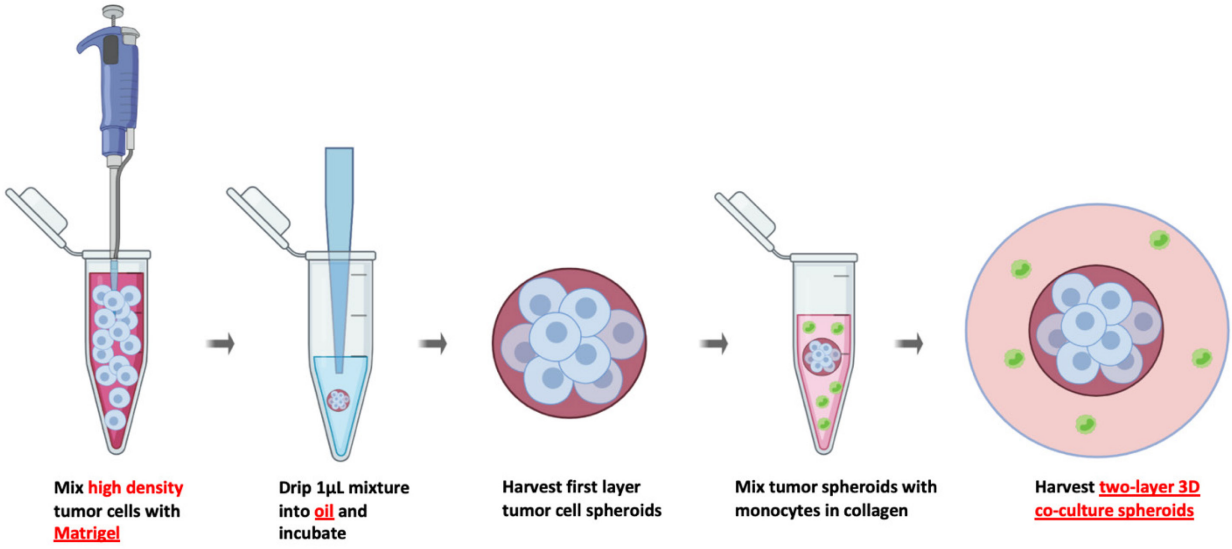

Figure S6: Scheme of 3D double-layer co-culture spheroid making. 80,000 MDA-MB-231 were embedded into 1μL matrigel core. Incubate for 1h before harvesting tumor matrigel cores. Embed relatively small number of monocytes (8000 and below) into second collagen layer of spheroids, 5μL as total volume. Incubate for 1h before harvesting complete co-culture spheroids. Put one spheroid in one well of a 96-well plate and add in 200μL fresh media. Take phase contrast images for all spheroids after every 24h and measure volume.

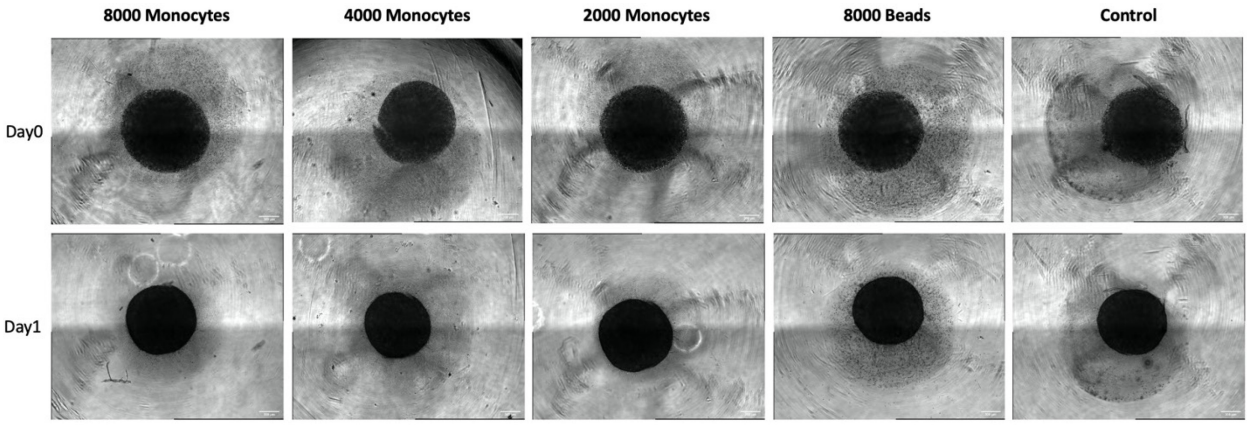

Figure S7: Primary monocyte spheroid contraction after 24 hours. Compared to spheroids with fresh DMEM and polystyrene beads in the outer collagen layer, spheroids with primary monocytes in the outer collagen layer showed smaller volume and faster contraction after only 24h incubation.

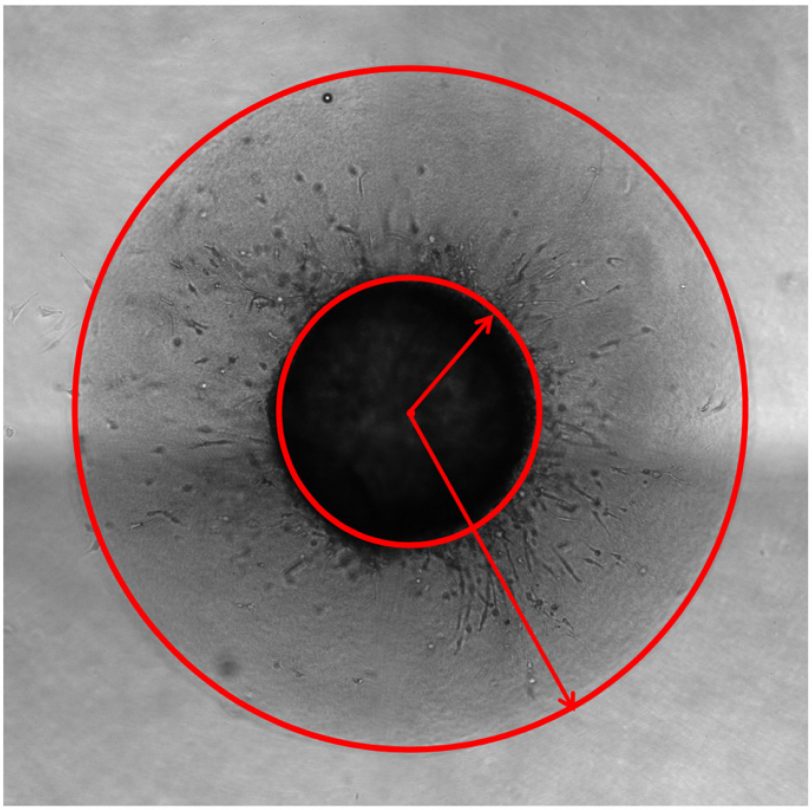

Figure S8: Measurement of spheroid volume. Manually trace the outer layers to generate radius measurement through NIS Elements software. Use this radius measurement to calculate the volume of total volume using $Volume = \frac{4}{3}\pi r^3$. Normalized volume for each day with initial day0 volume and thus getting a fraction number. Smaller numbers represent faster contraction rates. Notice in this image the elongated cells are invading MDA-MB-231 cells.

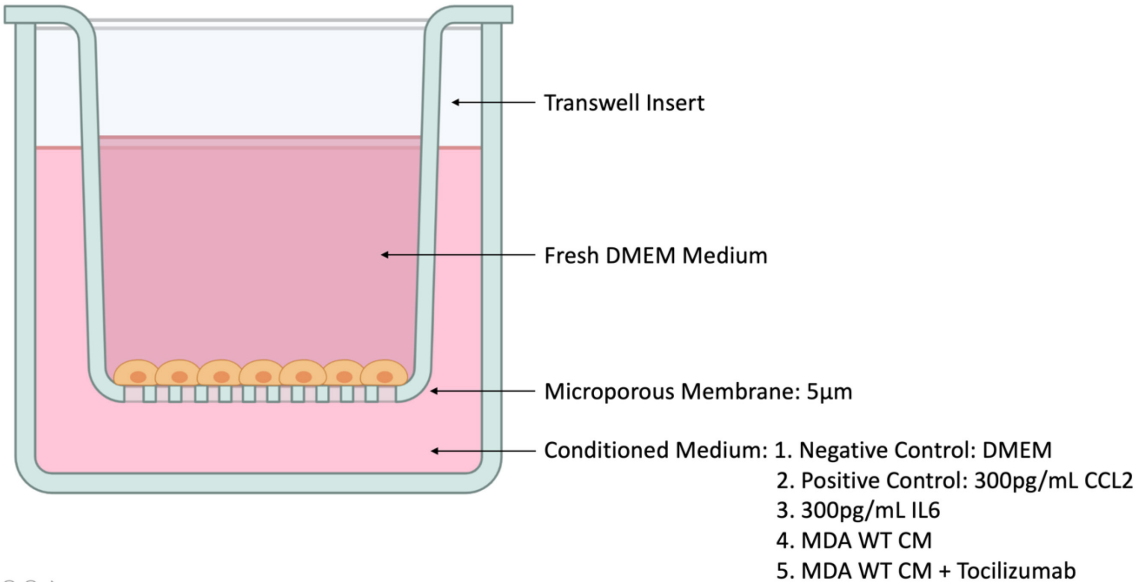

Figure S9: Scheme of transwell assay for cell biased migration (chemotaxis). Cells in fresh DMEM were seeded above the microporous membrane with a pore size of 5µm. Conditioned media were added to the bottom well. After a 6h incubation, cell numbers in the bottom well were measured.

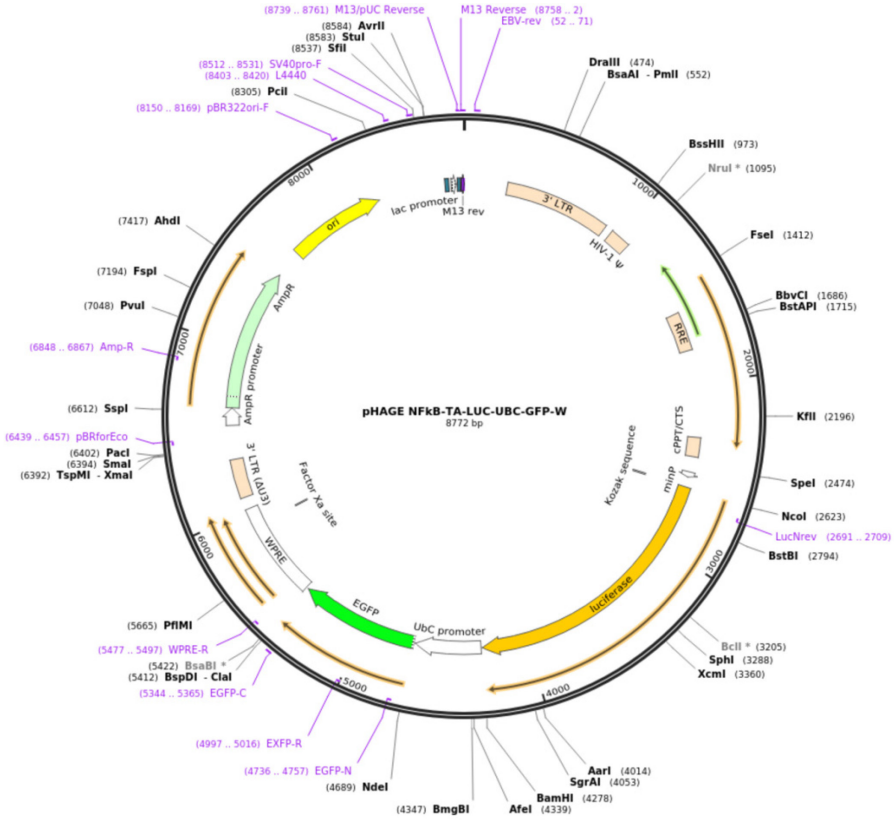

Figure S10: Structure of pHAGE NFkB-TA-LUC-UBC-GFP-W lentiviral vector.

References

1. Geissmann F, Manz MG, Jung S, Sieweke MH, Merad M, Ley K. Development of monocytes, macrophages, and dendritic cells. *Science*. 2010;327(5966):656-661.

2. Wynn T a., Chawla A, Pollard JW. Origins and Hallmarks of Macrophages: Development, Homeostasis, and Disease. *Nature*. 2013;496(7446):445-455.

3. Anbazhagan K, Duroux-Richard I, Jorgensen C, Apparailly F. Transcriptomic network support distinct roles of classical and non-classical monocytes in human. *Int Rev Immunol*. 2014;33(6):470-489.

4. Martinez FO, Gordon S. The M1 and M2 paradigm of macrophage activation: Time for reassessment. *F1000Prime Rep*. 2014;6(March):1-13.

5. Orekhov AN, Orekhova VA, Nikiforov NG, et al. Monocyte differentiation and macrophage polarization. *Vessel Plus*. 2019.

6. Honkanen TJ, Tikkanen A, Karihtala P, Mäkinen M, Väyrynen JP, Koivunen JP. Prognostic and predictive role of tumour-associated macrophages in HER2 positive breast cancer. *Sci Rep*. 2019;9(1):1-9.

7. Condeelis J, Pollard JW. Macrophages: Obligate partners for tumor cell migration, invasion, and metastasis. *Cell*. 2006;124(2):263-266.

8. Lin Y, Xu J, Lan H. Tumor-associated macrophages in tumor metastasis: Biological roles and clinical therapeutic applications. *J Hematol Oncol*. 2019;12(1):1-16.

9. Komohara Y, Fujiwara Y, Ohnishi K, Takeya M. Tumor-associated macrophages: Potential therapeutic targets for anti-cancer therapy. *Adv Drug Deliv Rev*. 2016;99:180-185.

10. Carey SP, Martin KE, Reinhart-King CA. Three-dimensional collagen matrix induces a mechanosensitive invasive epithelial phenotype. *Sci Rep*. 2017;7(February):1-14.

11. Grinnell F, Petroll WM. Cell Motility and Mechanics in Three-Dimensional Collagen Matrices. *Annu Rev Cell Dev Biol*. 2010;26(1):335-361.

12. Hsu BE, Roy J, Mouhanna J, et al. C3a elicits unique migratory responses in immature low-density neutrophils. *Oncogene*. 2020:2612-2623.

13. Frantz C, Stewart KM, Weaver VM. The extracellular matrix at a glance. *J Cell Sci*. 2010;123(24):4195-4200.

14. Kessenbrock K, Plaks V, Werb Z. Matrix Metalloproteinases: Regulators of the Tumor Microenvironment. *Cell*. 2010;141(1):52-67.

15. Jayatilaka H, Giri A, Karl M, et al. EB1 and cytoplasmic dynein mediate protrusion dynamics for efficient 3-dimensional cell migration. *FASEB J*. 2018;32(3):1207-1221.

16. Giri A, Bajpai S, Trenton N, Jayatilaka H, Longmore GD, Wirtz D. The Arp2/3 complex mediates multigeneration dendritic protrusions for efficient 3-dimensional cancer cell migration. *FASEB J*. 2013;27(10):4089-4099.

17. Jayatilaka H, Tyle P, Chen JJ, et al. Synergistic IL-6 and IL-8 paracrine signalling pathway infers a strategy to inhibit tumour cell migration. *Nat Commun*. 2017;8(May):1-12.

18. Wu PH, Giri A, Sun SX, Wirtz D. Three-dimensional cell migration does not follow a random walk. *Proc Natl Acad Sci U S A*. 2014;111(11):3949-3954.

19. Wu PH, Giri A, Wirtz D. Statistical analysis of cell migration in 3D using the anisotropic persistent random walk model. *Nat Protoc*. 2015;10(3):517-527.

Vita

Wenxuan DU

Mailing Add.: 500W University Pkwy, Apt 10G, Baltimore, MD, 21210
Contact: (Tel.) 410-900-2878 | E-mail: wdu8@jh.edu
Date of Birth: 05/23/1996

EDUCATION

Nankai University 09/2014 - 06/2018
Bachelor's degree received in 2018
Major: Pharmacy GPA: 90.39 Rank:1/68

University of California, Berkeley 07/2017 - 08/2017
Summer School
Courses: *Introduction to Functional Neuroanatomy* Grade: A+
Introduction to Human Physiology Laboratory Grade: A

Johns Hopkins University 08/2018 - present
Master of Science in Engineering expected in 2020
Major: Chemical & Biomolecular Engineering GPA: 3.94/4.0
TOEFL: 109 / GRE: 329+3.5

INTERNSHIP EXPERIENCE

Zhongjing Wanxi Pharmaceutical Co. Ltd. 07/2016 - 08/2016
- *Assistant of Quality Control Commissioner*
- Detected the extent of reaction and the product purity in silica gel chromatography in the lab using TLC (Thin-Layer Chromatography)
- Conducted impurity detection using HPLC (High Performance Liquid Chromatography) machine

RESEARCH EXPERIENCE

National University Student Innovation Project 05/2016 - 06/2018
- *Team leader & presenter*

Project Name: *Adjuvant Effective Nano Vaccine with TACAs (Tumor Associated Carbohydrate Antigen) for Cancer Curing Therapy*
Supervisor: Yanming Wang (Associate Professor at Nankai Univ.)
- Assembled a team of students. Led members to review extensive literature, summarized existing research results made by scientists, created a 10,000-word proposal and designed the experiment scheme.
- Received 30,000 RMB government grants.
- Delivered a 40-silde presentation to introduce our project in the final defense.

Graduate Research for MSE of Chemical & Biomolecular Engineering at JHU 09/2020 - present
- *Master candidate*

Project Name: *Bidirectional Regulation of Migration and Chemotaxis between Monocytes and Tumor Cells*
Supervisor: Dr. Denis Wirtz (Vice Provost for Research, Theophilus Halley Smoot Professor at JHU)

EXTRACURRICULAR EXPERIENCE

Science Department in the Student Union 09/2014-07/2016

- *Vice Minister*
- Took charge of department promotion like designing posters and issue-preparation.
- Organized tours for undergraduates in the National Key Laboratory of Medicinal Chemistry and Biology.
- Communicated with graduate lab leaders to enrich department activities and optimized management with the minister.

HONORS & AWARDS

- National Scholarship (8000RMB), Nankai Univ.	2/68	09/2016
- First-class Scholarship (5000 RMB), Nankai Univ.	5/68	2015 & 2017
- Merit Students, Nankai Univ.	7/68	2015 - 2017

SKILLS

Cell culture, 3D cell migration assay, Microscopy, Bacteria culture, DNA extraction, qPCR, Western Blot, Lentivirus transduction, Cryo-section, MATLAB, MetaMorph, Graphpad